Geoscience Frontiers xxx (2014) 1–29

HOSTED BY

Contents lists available at ScienceDirect

China University of Geosciences (Beijing)

Geoscience Frontiers

journal homepage: www.elsevier.com/locate/gsf

Research paper

The Sytykanskaya kimberlite pipe: Evidence from deep-seated xenoliths and xenocrysts for the evolution of the mantle beneath Alakit, Yakutia, Russia

I.V. Ashchepkov [a,*], A.M. Logvinova [a], L.F. Reimers [a], T. Ntaflos [b], Z.V. Spetsius [c], N.V. Vladykin [d], H. Downes [e], D.S. Yudin [a], A.V. Travin [a], I.V. Makovchuk [d], V.S. Palesskiy [a], O.S. Khmel'nikova [a]

[a] Institute of Geology and Mineralogy SB RAS, Koptyug ave 3, Novosibirsk 630090, Russia
[b] Vienna University, A-1090 Vienna, Austria
[c] Alrosa Stock Company, Lenina 6, Mirny, Russia
[d] Institute of Geochemistry SB RAS, Favorsky 1a, Irkutsk 664033, Russia
[e] Birkbeck College, University of London, UKMalet Street, Bloomsbury, London WC1E 7HX, UK

ARTICLE INFO

Article history:
Received 21 May 2014
Received in revised form
31 July 2014
Accepted 4 August 2014
Available online xxx

Keywords:
Kimberlites
Mantle lithosphere
Mantle xenoliths
Thermobarometry
Pyropes

ABSTRACT

Mantle xenoliths (>150) and concentrates from late autolithic breccia and porphyritic kimberlite from the Sytykanskaya pipe of the Alakit field (Yakutia) were analyzed by EPMA and LAM ICP methods. In P-T-X-$f(O_2)$ diagrams minerals from xenoliths show widest variations, the trends P-Fe$^{\#}$-CaO, $f(O_2)$ for minerals from porphyric kimberlites are more stepped than for xenocrysts from breccia. Ilmenite PTX points mark moving for protokimberlites from the lithosphere base (7.5 GPa) to pyroxenite lens (5–3.5 GPa) accompanied by Cr increase by AFC and creation of two trends P-Fe$^{\#}$Ol ~10–12% and 13–15%. The Opx-Gar-based mantle geotherm in Alakit field is close to 35 mW/m^2 at 65 GPa and 600 °C near Moho was determined. The oxidation state for the megacrystalline ilmenites is lower for the metasomatic associations due to reduction of protokimberlites on peridotites than for uncontaminated varieties at the lithosphere base. Highly inclined linear REE patterns with deep HFSE troughs for the parental melts of clinopyroxene and garnet xenocrysts from breccia were influenced by differentiated protokimberlite. Melts for metasomatic xenoliths reveal less inclined slopes without deep troughs in spider diagrams. Garnets reveal S-shaped REE patterns. The clinopyroxenes from graphite bearing Cr-websterites show inclined and inflected in Gd spectrums with LREE variations due to AFC differentiation. Melts for garnets display less inclined patterns and Ba-Sr troughs but enrichment in Nb-Ta-U. The $^{40}Ar/^{39}Ar$ ages for micas from the Alakit mantle xenoliths for disseminated phlogopites reveal Proterozoic (1154 Ma) age of metasomatism in early Rodinia mantle. Veined glimmerites with richterite – like amphiboles mark ~1015 Ma plume event in Rodinia mantle. The ~600–550 Ma stage manifests final Rodinia break-up. The last 385 Ma metasomatism is protokimberlite-related.

1. Introduction

The Sytykanskaya kimberlite pipe of the Yakutian kimberlite province is located near the boundary of the Daldyn and Alakite fields (Fig. 1A) in the upper stretches of the Sytykan creek (Fig. 1B) (Sobolev, 1977; Spetsius and Serenko, 1990; Ashchepkov et al., 2010). It is buried by dolerite sills up to 70 m in thickness. The pipe is built up from two independent bodies: northeast (main) consisting from early breccia and porphyric kimberlite (PK) and late autolithic kimberlite breccia (ABK) and southwest body compiled

* Corresponding author. Sobolev's Institute of Geology and Mineralogy SD RASc, Academician V.A. Koptyug Avenue 3, 63090 Novosibirsk, Russia. Tel.: +7 950 5918327; fax: +7 950 5918327, +7 383 2332792 (institute).
E-mail addresses: Igor.Ashchepkov@igm.nsc.ru, garnet@igm.nsc.ru, igora57@mail.ru (I.V. Ashchepkov).
Peer-review under responsibility of China University of Geosciences (Beijing).

http://dx.doi.org/10.1016/j.gsf.2014.08.005

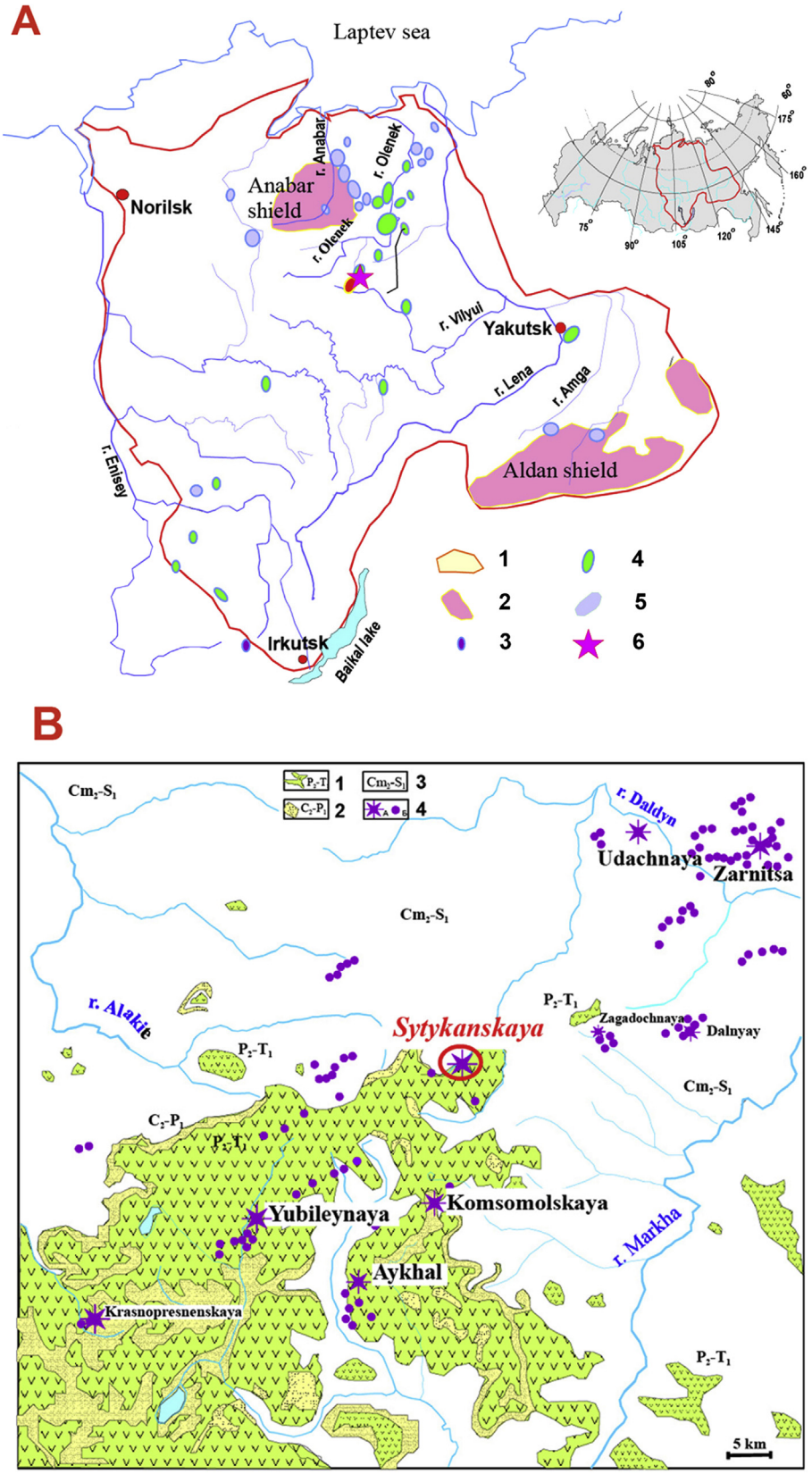

Figure 1. (A) Location of Sytykanskaya pipe Alakit field and other kimberlite fields in Siberian platform. 1—Siberian platform; 2—Shields, Kimberlite fields; 3—Alakit field, late Devonian fields; 4—Low Triassic and Jurassic fields (Kostrovitsky et al., 2007). 5—kimberlite fields; 6—location of Sytykan pipe. (B) Geological scheme of the Alakite pipe and location of the kimberlite pipes. 1—P_2-T_1 trap dolerites; 2—C_2-P_1 sandstones; 3—Cm_2-S_1; 4—kimberlite pipes excavated (a) and buried (b).

Please cite this article in press as: Ashchepkov, I.V., et al., The Sytykanskaya kimberlite pipe: Evidence from deep-seated xenoliths and xenocrysts for the evolution of the mantle beneath Alakit, Yakutia, Russia, Geoscience Frontiers (2014), http://dx.doi.org/10.1016/j.gsf.2014.08.005

by breccia. There are three phases of the kimberlite intrusion. All kimberlites types in Sytykan pipes are more abundant in ilmenites and pyropes than other pipes from the Daldyn–Alakite region. The main ABK body contain smaller portion of pyrope and higher picroilmenite, than porphyric kimberlites and early breccia. In breccia from southwest body pyrope content is lower than in the main northeastern body. Mantle xenoliths are rare in southwest body but compile to 3.5 vol.% in ABK in central part where ultramafic xenoliths prevail and some diamondiferous eclogites were found also (Koptil et al., 1975; Ponomarenko and Spetsius, 1976; Lazko et al., 1982; Spetsius, 2007; Spetsius and Koptil, 2008). The ABK differs from northeastern PK by higher amount of dunites, garnet-spinel lherzolites. The early phases contain some cataclastic lherzolites, ilmenite-bearing peridotites and granular-grained garnet lherzolites as well as Cr-diopside pyroxenites. The Sytykanskaya pipe reveals sharp difference in diamond grade and different typomorphic features of diamonds in different kimberlite portions. Diamond grade in early breccia and PK of northeastern body are less in 7 times comparing with those of the ABK (Spetsius and Serenko, 1990; Spetsius and Koptil, 2008). The kimberlite in this pipe is now completely excavated and is lying near the pipe. The diamond grade is not very high compared with the other large pipes in the Alakit field but some large diamonds to 342 carats were discovered.

Among the kimberlites from Alakit field, the Sytykanskaya pipe is characterized by a large amount of deep-seated xenoliths which contain relics of fresh minerals, e.g. clinopyroxenes (Cpx), garnets (Gar), olivines (Ol), phlogopites (Phl), amphiboles (Amph), chromites (Chr), ilmenites (Ilm) and some other rare phases.

In this work we give the characteristics of the deep-seated xenoliths and xenocrysts from this pipe using mainly EPMA and ICP MS analyses and compare these results with the data for the concentrates from ABK and PK on the variation and P-T-X-$f(O_2)$ diagrams.

The xenocrysts of ABK, PK and minerals from xenoliths were analyzed and plotted separately to see the difference and the evolution of the mantle roots and feeder systems of the protokimberlites. The comparison of the compositional fields for the minerals from xenoliths and concentrates in the Hacker's variation diagrams allow to recognize the details of the variations and grouping and find out their origin which is also useful for the estimation of the potential diamond grade.

2. Methods and data

The minerals from the concentrates of ABK (~500) and PK (~400) from Sytykanskaya pipe were analyzed by electron probe microanalysis (EPMA). About 160 peridotite xenolths of lherzolite, mainly veined lherzolites and enriched harzburgite type, half of which contain veins with phlogopites and other metasomatic minerals, and 10 pyroxenites and several eclogites mostly from breccia were also analyzed with Camebax Micro microprobe using the methods described in the published paper (Lavrent'ev et al., 1987). For the compilation of diagrams we also used the set of minerals from ~50 xenoliths and ~200 diamond inclusions analyzed by the same technique from the dissertation of L Reimers (1994) and published data for the eclogite diamond bearing associations (Spetsius, 2007; Spetsius and Koptil, 2008) (Supplement 3). The most interesting xenoliths (15) were analyzed in detail in the University of Vienna in thin section using Camaca100 SX microprobe.

Analyses of trace elements for three types of inclusions: xenocrysts from the breccia concentrate, metasomatic and veined xenoliths and garnet websterites, were obtained by LAM-ICPMS methods using Finnigan Element mass spectrometer and laser ablation system Nd YAG: UV NewWave in Analytic Center of IGM SD RAS (Tables 1–3).

The phlogopite grains from xenoliths and xenocrysts from kimberlites were analyzed for $^{40}Ar/^{39}Ar$ age using the method described in detail in the previous publication (Travin et al., 2009). The quartz ampoules with samples were irradiated in the Cd-coated channel of a reactor (BBP-K type) at the Tomsk Polytechnic Institute. The gradient of the neutron flux did not exceed 0.5% of the sample size. The experiments on the stepwise heating were carried out in a quartz reactor with an external heater. The blank for ^{40}Ar (10 min at 1200 °C) was no higher than 5×10^{-10} ncm^3. Ar was purified using Ti and ZrAl SAES getters. The isotopic composition of Ar was measured on a Noble Gas 5400 (Micromass, United Kingdom) mass spectrometer.

3. Petrography

Collection of about 300 xenoliths was used to determine the variations of the petrographic groups in the mantle section beneath the Sytykan pipe. The xenoliths are represented by slightly depleted garnet lherzolites (Fig. 2A, B, I, N) (35%) and harzburgites (10%) (Fig. 2E, F), Sp lherzolites (10%) (Fig. 2G), deformed peridotites (3%) (Fig. 2C), Ilm-bearing peridotites where Ilm is rock forming mineral (Fig. 2J, O), garnet phlogopite-ilmenite veined peridotite xenoliths (Fig. 2F, G, L, I) (15%), garnet (Fig. 2G) and Chr dunites (4%), garnet pyroxenites (Fig. 3A–D) with ilmenites graphite and mica (7%), and Phl-Ilm metasomatic veins (glimmerites) (8%) (Fig. 2C) and relatively low amount of eclogites (Fig. 3E–F) (<0.2). The percentage of the rock type among the xenoliths is similar to those reported in previous works (Bobrievich et al., 1959; Spetsius and Serenko, 1990; Manakov, 2001).

Most of peridotite xenoliths contain phlogopite (Fig. 2E–O) as well as pyroxenites and eclogites. It is found as sporadic grains dispersed in the rocks and also as micro- and macro-veins, commonly with Cr-diopsides and more rarely garnet or chromite. Phlogopites commonly form coronas on garnets (Fig. 2D, K) or together with pyroxenes and chromites totally replace garnets grains, forming symplectites or complex intergrowth of Cpx, Phl, Chr (Fig. 2C, K) and rarely secondary garnets (Fig. 2K) (see Supplement File 1). Veins of Ilm-Phl-Cr-diopsides form the stockworks in the peridotite matrix (Fig. 2L) and cut through the large porphyroclusts of olivine and garnets. Sometimes they are very thin and even dispersed. But in other cases the ilmenites built up to 5–10% of rock volumes (Fig. 2O) which happens commonly near the contacts with the megacrystalline associations. Some Ilm-Cpx or monomineral ilmenite veins cut large garnet porphyroclasts. Rare xenoliths of fine-grained essentially olivine peridotites contain intergranular Ilm and ulvospinel grains as well as Cr-diopsides (Cr-Di) and garnet relics. They are relatively low temperature analogs of the deformed peridotites (Boyd et al., 1997; Ionov et al., 2010; Agashev et al., 2013). Eclogite xenoliths rarely occur in other Yakutian kimberlite pipes (Sobolev et al., 1984; Spetsius and Serenko, 1990; Pearson et al., 1995; Snyder et al., 1997; Misra et al., 2004; Pernet-Fisher et al., 2014), and we have analyzed two samples in our study (Fig. 3E, F); though some diamond-bearing eclogites were discovered in this pipe (Spetsius and Serenko, 1990). And some of them contain kyanite also (Koptil et al., 1975). Several practically fresh garnet pyroxenites-websterites which also contain mica and chromites, were found in PK (Fig. 3A–D). Some of them contain significant amounts of graphite (Fig. 4C).

The megacryst association is represented mainly by ilmenite (Supplement File 1, Fig. 2A) and pyrope garnets. Several large ilmenite nodules represent large monocrystals cemented by fine Ilm grains and, in the outer contact, these aggregates contain Cr-Di and olivines typical for peridotites. These types of xenoliths are close to the contacts of the Ilmenite polycrystalline nodules with deformed peridotites (Moore and Lock, 2001).

Please cite this article in press as: Ashchepkov, I.V., et al., The Sytykanskaya kimberlite pipe: Evidence from deep-seated xenoliths and xenocrysts for the evolution of the mantle beneath Alakit, Yakutia, Russia, Geoscience Frontiers (2014), http://dx.doi.org/10.1016/j.gsf.2014.08.005

Table 1
Compositions of the mantle xenocrysts from the Sytykan kimberlite pipes breccia (Major elements are in in wt.% and trace elements in ppm).

Element	S079	S052	S053	S054	S055	S056	S068	S640	S068	S067	S053	STK14	STK24	STK137	SG76	SG07	SG78	SG79	SG66	SG87	SG60	SG62	SG63	SG64	SI169	SI149	SI150	SI135	SI123	SI138	SI152
	Clinopyroxenes											Phlogopites			Garnets										Ilmenites						Ulvo-spinel
SiO_2	54.89	55.25	55.29	54.55	55.90	55.43	52.72	55.48	54.90	55.13	55.46	42.70	42.35	42.75	41.51	40.84	42.05	41.56	40.84	42.06	42.06	41.71	40.8	42.29							
TiO_2	0.13	0.12	0.13	0.14	0.08	0.30	0.42	0.08	0.10	0.13	0.23	0.37	0.43	0.37	0.193	0.161	0.232	0.218	0.161	0.678	0.678	0.15	0.133	0.064	53.69	50.68	49.18	49.13	46.93	53.09	49.38
Al_2O_3	2.03	0.43	0.70	0.74	3.22	3.31	2.51	0.78	0.54	2.37	1.64	11.02	11.98	10.84	21.22	15.53	22.24	21.39	15.53	16.34	16.34	21.01	19.91	21.75	0.68	0.25	0.35	0.32	0.34	0.53	0.33
Cr_2O_3	2.36	1.74	0.65	3.19	5.35	3.56	3.26	2.54	3.42	2.76	0.13	0.21	0.38	0.20	2.33	9.95	0.766	2.38	9.95	5.87	5.87	3.01	3.98	3.37	0.65	0.95	1.89	1.93	2.63	4.93	1.80
FeO	2.66	3.43	1.82	1.65	2.06	3.16	2.92	2.56	2.05	2.56	3.91	3.60	2.70	3.41	7.73	7.03	9.01	8.8	7.03	7.91	7.91	9.13	9.33	7.45	31.60	35.80	37.32	38.63	39.35	24.46	38.30
MnO	0.09	0.07	0.07	0.06	0.09	0.08	0.10	0.06	0.06	0.09	0.06	0.02	0.03	0.01	0.334	0.427	0.479	0.482	0.427	0.334	0.334	0.496	0.521	0.49	0.24	0.26	0.35	0.28	0.32	0.32	0.34
MgO	15.89	16.28	17.04	16.11	13.50	14.53	15.84	16.23	15.70	15.59	17.16	27.79	26.98	28.08	20.16	20.06	16.34	20.17	20.06	20.01	20.01	20.26	18.04	22.06	12.06	10.35	10.60	9.52	8.59	16.25	9.29
CaO	19.81	22.86	23.32	21.29	17.19	16.64	21.06	21.20	21.54	18.94	21.82	0.05	0.02	0.11	4.74	4.86	8.17	3.92	4.86	4.59	4.59	3.74	6.02	2.97							
Na_2O	2.71	1.69	0.58	1.81	4.46	4.21	1.99	2.19	2.23	3.09	1.40	0.18	0.12	0.13	0.049	0.049	0.038	0.065	0.049	0.236	0.236	0.041	0.017	0.033							
K_2O												10.24	9.55	9.46																	
Total	100.57	101.88	99.60	99.55	101.85	101.22	100.83	101.12	100.54	100.66	101.82	96.18	94.53	95.36	98.27	98.91	99.33	98.99	98.91	98.03	98.03	99.55	98.75	100.48	98.92	98.28	99.68	99.81	98.16	99.59	99.44
Ba	3.67	0.59	7.6	0.66	15.71	12.24	0.68	0.97	0.97	6.31	0.29	21546	16128	22.82	4.44	3.14	7.27	0.91	1.93	3.06	0.03	0.12	2.16	4.07	12.24	0.22	0	0.15	0.02	58.76	404.8
La	1.72	8.8	9.34	3.25	16.39	45.02	31.01	38.98	45.26	116.82	5.97	3.6	0.59	1.7	0.97	0.11	0.73	0.1	0.71	0.13	0.02	0.06	0.59	0.37	4.53	0.13	0.008	0.011	0.012	69.98	17.59
Ce	5.1	35.3	28.8	12.9	36.3	113.7	106.2	136.1	178	299.2	11.3	6.72	1.69	6.56	0.56	0.82	2.78	1.04	2.74	1.3	0.12	0.47	2.08	1.45	9.31	0.827	0.015	0.023	0.078	74.52	28.98
Pr	0.8	5.9	4.7	2	5	15.2	11.2	14.1	18.2	34.9	1.5	0.79	0.32	0.82	0.23	0.44	0.38	0.23	0.49	0.17	0.03	0.07	0.56	0.18	1.28	0.049	0.006	0.002	0.008	5.7	2.12
Nd	4.5	28.3	23.7	9.2	22.1	66.1	44.5	52.8	65.1	131.7	5.4	5.22	2.96	4.76	3.13	4.06	1.69	1.93	2.75	1.04	0.29	0.35	4.04	1.47	5.72	0.256	0.057	0.009	0.049	18.71	9.13
Sm	1.05	5.72	5.18	1.87	4.28	12.25	8	9.81	11.81	20.73	0.44	2.58	0.9	0.8	1.22	1.42	0.46	1.5	0.98	0.86	0.29	0.12	0.9	1.37	0.67	0.072	0.026	0.007	0.016	2.36	1.13
Eu	0.39	1.64	1.55	0.53	1.11	3.44	2.48	3.03	3.34	6	0.12	0.6	0.3	0.17	0.53	0.31	0.09	0.62	0.39	0.06	0.17	0.06	0.2	0.55	0.13	0.016	0.007	0.003	0.003	0.58	0.29
Gd	1.11	4.28	4.18	1.38	3.78	10.36	5.89	6.77	7.82	13.81	0.3	0.44	0.47	0.47	2.51	0.65	0.24	2.57	1.32	0.14	0.6	0.24	0.57	2.93	0.24	0.058	0.014	0.024	0.021	1.68	0.61
Tb	0.14	0.43	0.43	0.14	0.45	1.1	0.66	0.77	0.87	1.56	0.03	0.03	0.06	0.04	0.83	0.07	0.02	0.5	0.15	0.04	0.16	0.09	0.09	0.66	0.03	0.007	0.004	0.004	0.009	0.19	0.09
Dy	0.84	2.05	1.97	0.6	1.88	4.92	2.87	3.48	3.64	6.33	0.13	0.12	0.18	0.15	6.93	0.4	0.07	3.79	0.53	0.31	1.35	1.02	1.13	5.71	0.15	0.04	0.041	0.029	0.021	0.99	0.39
Ho	0.14	0.29	0.28	0.09	0.31	0.68	0.37	0.45	0.47	0.91	0.02	0.03	0.03	0.03	2.1	0.07	0.02	0.92	0.08	0.1	0.37	0.34	0.38	1.35	0.03	0.008	0.013	0.005	0.003	0.17	0.05
Er	0.34	0.65	0.56	0.18	0.71	1.08	0.7	0.82	0.84	1.57	0.03	0.08	0.05	0.23	5.37	0.17	0.09	2.72	0.2	0.39	1.06	1.49	1.61	4.69	0.08	0.024	0.012	0.016	0.019	0.41	0.11
Tm	0.04	0.06	0.06	0.02	0.08	0.12	0.06	0.08	0.09	0.18	0.003	0.02	0.02	0.02	0.75	0.05	0.01	0.41	0.04	0.07	0.19	0.27	0.29	0.74	0.01	0.003	0.005	0.003	0.008	0.06	0.03
Yb	0.22	0.4	0.31	0.1	0.48	0.66	0.32	0.38	0.44	0.83	0.011	0.06	0.11	0.36	5.4	0.28	0.23	3.06	0.38	0.81	1.4	2.17	2.98	5.85	0.1	0.032	0.026	0.034	0.022	0.45	0.1
Lu	0.03	0.04	0.03	0.01	0.06	0.06	0.04	0.04	0.05	0.09	0.002	0.01	0.04	0.08	0.85	0.11	0.03	0.49	0.12	0.15	0.23	0.39	0.59	0.88	0.02	0.005	0.007	0.007	0.005	0.05	0.02
Hf	0.56	2.43	3.14	1.04	5.7	6.93	1.92	2.35	2.42	4.43	0.37	0.35	0.22	0.17	0.7	0.26	0.13	2.26	0.64	0.11	0.57	0.11	0.54	1.96	28	17	17	28	26	37	45
Ta	0.03	0.11	0.17	0.02	0.34	0.15	0.03	0.04	0.2	4.06	0.002	0.61	3.77	1.12	0.01	0.07	0.05	0.06	0.05	0.11	0.01	0.02	0.21	0.09	431	269	183	377	364	373	18
Pb	2.84	0.29	0.71	0.33	10.44	5.86	2.77	3.72	4.12	4.77	0.8	9.96	1.92	1.73	0.77	0.84	1.75	0.35	0.73	1.05	0.22	0.27	1.73	2.83	6.36	1.67	0.18	0.99	0.59	14.02	7.88
Th	0.09	0.1	0.62	0.03	1.07	2.43	1.76	2.37	2.32	10.06	0.46	10.58	4.44	0.47	0.04	0.27	0.3	0.02	0.12	0.03	0.03	0.02	0.15	0.05	0.25	0.01	0.005	0.002	0.001	7.54	1.33
U	0.06	0.03	0.18	0.01	0.82	0.28	0.35	0.53	0.5	1.01	0.02	0.34	0.53	8.84	0.02	0.04	0.04	0.03	0.07	0.05	0.01	0.02	0.1	0.11	0.34	0.08	0.04	0.05	0.04	3.8	0.87
Sc	20	47	45	15	196	186	109	143	144	199	12	42	21	15	108	107	8	143	259	136	42	125	463	156	64.4	32.5	31.7	40.7	39.7	64.4	14
V	182	155	376	187	348	1084	1236	1649	1637	1462	141	1897	634	2151	217	102	1412	476	628	435	74	386	778	371	2826	2110	1809	1801	1840	1994	1466
Co	34	7	18	9	119	72	76	100	103	101	5	1023	490	539	41	23	408	93	106	68	22	71	107	118	331	270	222	196	202	272	42
Cu	5.46	0.18	6.56	1.05	52.71	16.51	2.53	6.42	2.16	11.66	0.3	33	18	13	180	202	78	3.3	7.5	14.1	1	0.7	10.1	23.4	59	55	47	34	30	84	34
Ni	434	114	317	126	2524	1014	957	1257	1253	1566	85	7548	4607	849	286	192	437	169	104	119	47	66	226	505	1370	1015	935	1030	1256	1958	329
Rb	0.73	0.04	0.63	0.05	3.81	0.32	0.01	0.02	0.07	0.4	0.03	7.56	3.38	7.35	0.05	0.1	3.5	0.01	0.14	0.52	0.06	0.11	0.15	0.39	5.22	0.21	0.03	0.33	0.14	28.2	2.37
Sr	102	247	253	119	415	968	770	979	1042	1318	133	50	21	389	0	2.56	194.57	1.75	126	3.9	1.32	0.54	8.42	11.78	70.8	6.4	0.4	0.5	0.5	147.4	38.3
Y	3.35	7.02	6.25	2.05	7.71	15.8	9.11	10.54	11.46	19.87	0.36	568	587	6	2.8	1.9	3.7	22.6	1.9	2.6	8.9	10.5	11.1	36.3	5.75	0.22	0.16	0.11	0.11	4.17	14.8
Zr	4.47	35.1	41.3	13.8	115.9	143.7	52.4	64.6	75.5	148.6	3.19	49	43	54	58.5	32	34.8	80	36.7	4.6	19.3	2.9	17.1	70.3	408	417	417	760	764	1009	601
Nb	0.26	0.73	2.24	0.18	3.57	3.04	1.3	1.78	5.29	168.22	0.03	4.3	69	14	2.71	2.03	1.7	0.58	0.69	1.26	0.05	0.31	1.74	0.72	3477	2005	1264	2708	2478	2929	204

Table 2
Compositions of the minerals from the peridotite mantle xenoliths of Sytykan kimberlite pipe (Major elements are in in wt.% and trace elements in ppm).

Number	STK174	STK184	Stk148	STK139	Stk197	Stk215	STK15	STK21	Stk144	STK169	STK15	S64	S15	S7	S55
Element	Clinopyroxenes								Garnets				Phl	Ilmenites	
SiO_2	55.94	55.74	54.76	55.24	56.05	55.25	54.52	55.01	41.45	42.06	41.71	42.10	43.15		
TiO_2	0.31	0.173	0.244	0.148	0.19	0.43	0.146	0.272	0.04	0.09	0.14	0.02	0.30	51.61	45.66
Al_2O_3	2.28	2.32	3.43	3.84	2.58	4.93	2.76	1.47	16.23	18.85	21.33	18.13	11.61	0.02	0.38
Cr_2O_3	1.66	0.454	4.54	4.24	3.31	2.63	1.47	1.21	9.56	5.75	3.00	6.01	0.44	3.18	3.05
FeO	2.47	3.07	2.04	2.26	2.41	1.80	2.78	3.58	6.71	7.80	7.71	8.22	3.59	33.17	39.69
MnO	0.06	0.053	0.088	0.078	0.08	0.08	0.076	0.108	0.41	0.47	0.37	0.46	0.01	0.46	0.21
MgO	15.53	17.69	13.62	12.69	15.22	13.27	16.96	19.27	22.45	20.57	20.12	20.78	26.02	11.55	9.66
CaO	19.60	18.37	16.23	16.23	17.44	17.16	17.95	16.16	2.19	5.10	4.21	3.73	0.01		
Na_2O	2.38	2.28	4.23	4.61	3.55	4.15	3.12	1.56	0.06	0.08	0.05	0.01	0.11		
K_2O	0.02	0.01	0.03	0.03	0.01	0.03	0.01	0.06	0.00	0.00	0.00	0.01	9.79		
Total	100.24	100.16	99.21	99.37	100.84	99.73	99.79	98.70	99.10	100.76	98.65	99.47	95.03	100.00	98.66
Ba	2.04	2.61	6.77	8.23	3.55	7.16	4.55	1.29	0.38	0.94	0.52	1.39	2.52	1.37	73.27
La	3.82	9.51	16.14	1.07	3.04	1.80	5.41	3.63	0.007	0.085	0.098	0.03	0.171	0.344	2.94
Ce	10.6	27.8	41.0	2.73	8.99	4.29	19.06	6.76	0.072	0.32	0.001	0.15	0.601	0.616	4.88
Pr	1.582	4.387	5.718	0.295	1.174	0.914	2.008	1.24	0.085	0.044	0.002	0.01	0.006	0.168	0.383
Nd	6.94	20.46	21.59	1.30	6.46	2.44	8.81	6.13	0.56	0.25	0.21	0.12	0.225	0.33	1.61
Sm	2.16	4.29	3.03	0.25	1.42	0.36	1.83	1.58	0.12	0.01	0.05	0.12	0.001	0.34	0.26
Eu	0.48	1.15	0.67	0.03	0.41	0.12	0.68	0.37	0.03	0.00	0.05	0.016	0.007	0.01	0.04
Gd	1.54	3.09	1.45	0.12	1.10	0.29	1.80	1.35	0.07	0.31	0.22	0.014	0.006	0.001	0.062
Tb	0.195	0.334	0.151	0.006	0.103	0.03	0.18	0.15	0.003	0.004	0.079	0.009	0.001	0.002	0.011
Dy	1.21	1.42	0.61	0.09	0.54	0.09	0.79	0.73	0.043	0.002	0.672	0.138	0.007	0.015	0.056
Ho	0.158	0.26	0.066	0.011	0.087	0.023	0.155	0.098	0.009	0.001	0.21	0.04	0.003	0.006	0.009
Er	0.24	0.45	0.19	0.008	0.212	0.033	0.373	0.215	0.017	0.007	0.55	0.13	0.073	0.005	0.014
Tm	0.023	0.07	0.012	0.011	0.038	0.018	0.038	0.017	0.005	0.002	0.07	0.014	0.002	0.003	0.001
Yb	0.163	0.402	0.071	0.071	0.074	0.012	0.171	0.052	0.021	0.014	0.57	0.22	0.037	0.027	0.011
Lu	0.01	0.053	0.005	0.002	0.011	0.005	0.046	0.006	0.011	0.002	0.08	0.03	0.001	0.001	0.005
Hf	1.71	2.49	0.61	0.137	3.876	0.34	0.696	1.167	0.031	0.016	0.07	0.05	0.015	2.806	7.42
Ta	0.009	0.10	0.12	0.21	0.03	0.18	0.34	0.007	0.006	0.004	0.0003	0.002	0.1	39.041	2.65
Pb	0.30	0.23	1.10	0.55	0.90	0.68	1.54	0.34	0.03	0.15	0.049	0.06	0.15	0.604	1.23
Th	0.044	0.307	0.411	1.5	0.168	0.358	0.769	0.106	0.033	0.038	0.004	0.025	0.048	0.025	0.225
U	0.008	0.024	0.12	0.14	0.02	0.03	0.13	0.003	0.004	0.004	0.002	0.005	0.843	0.032	0.138
Sc	19.02	45	16	3	171	7.9	25.0	16.04	13.03	0.48	10.23	21.4	0.69	5.75	1.79
V	236	133	256	942	336	705	129	187	13	185	23	25	226	297	256
Co	3.9	7.55	8.69	135	80	137	93	3.00	2.76	51.4	4.20	4.99	54.3	33.3	6.96
Cu	1.01	5.45	7.69	5.82	2.94	6.32	6.93	2.22	25.67	9.42	18.27	0.54	0.83	5.61	5.02
Ni	40	67	227	628	1427	808	1446	36	10	70	17	17	81	139	70
Rb	0.10	0.88	0.81	2.63	1.07	1.25	9.53	0.04	0.03	0.21	0.08	0.05	0.33	0.32	1.87
Sr	352	225	70	3.98	162	14.134	20.5	246	0.12	0.38	0.23	1.97	0.69	1.87	2.38
Y	3.53	5.39	1.79	0.36	2.32	0.76	5.70	2.42	0.18	0.02	4.73	1.04	0.03	0.06	0.17
Zr	15.11	33.25	7.28	1.90	32.51	3.61	10.02	9.52	0.49	0.83	1.26	0.25	0.30	41.00	112.20
Nb	0.38	0.94	1.55	3.38	0.69	3.53	7.35	0.00	0.01	0.00	0.00	0.00	1.14	377.89	36.72

4. Mineralogy

Pyrope compositions on the diagram for the breccia and xenoliths (Fig. 4A) and porphyritic kimberlites and pyroxenites (Fig. 4B) show similarity in the configuration of the clusters and close interval of Cr_2O_3 variations to 13%. The total amount of sub-Ca garnets in PK (Sobolev, 1977; Pokhilenko et al., 1991; Sobolev et al., 2003, 2004) is higher. The largest fraction of Ti-rich garnets plots in the part of the left diagrams, as well as CaO-rich garnets of pyroxenitic type and Fe-enriched from the metasomatites in the middle part of the diagram. In the P-$Fe^{\#}$ and P-CaO diagrams (Figs. 10–12) the trends for garnets from the ABK and metasomatic xenoliths are more complex possibly due to significance of interaction during the metasomatic processes. The garnets from PK reveal more straight and stepped trends in variation diagrams.

The Cr-diopsides on the variation diagrams (Fig. 5) divide into three intervals according to FeO content. Most of them belong to low-Fe type (1–2.5 wt.% FeO) and low contents of all admixtures including Cr which slightly increases with FeO, come from enriched harzburgites and lherzolites. The Cr-Di varieties showing greatest variability Na, Cr, Al, Ti represent the metasomatic veins in the peridotites from the middle part of diagram (2–3.5 wt.% FeO). The highest values refer to Cr-Di from glimmerites with alkali amphibole close to richterite (Hawthorne and Oberti, 2007). The garnet websterites with mica contain clinopyroxenes with Cr_2O_3 <2 wt.%. The Fe-rich part corresponds to the Ilm-bearing metasomatites which reveal quite different Al_2O_3 and TiO_2 content.

Chromites are represented mostly by Cr-rich varieties (Fig. 6). The fraction of the varieties with Cr_2O_3 >62 wt.% that locate within the diamond window (Sobolev et al., 1973; Pokhilenko and Sobolev, 1995) is higher in the ABK and slightly less in the PK due to lower number of analyzed grains. But chromites from concentrates are enriched in TiO_2 comparing to grains from xenoliths. Amount of such chromites is higher in the metasomatic xenoliths. The Al_2O_3-Cr_2O_3 chromite plot does not show the common linear correlation but creates a cloud of points in the Cr-rich part explained by high degree of metasomatism. Only harzburgitic chromites from xenoliths form common Al_2O_3-Cr_2O_3 trend showing less metasomatic enrichments.

Imenites from Sytykanskaya pipe reveal the greatest variations (Fig. 7A, B) and most complicated trends among those studied in the Yakutian province (Ashchepkov et al., 2010, 2013a,b,c), showing wide variations in Cr and Al and other minor components. For the ilmenites from the porphyritic kimberlite there are 3 main levels of Cr_2O_3 enrichment. In Daldyn region three levels of Cr_2O_3 are common (Ashchepkov, 1980; Amshinsky, Pokhilenko, 1983;

Please cite this article in press as: Ashchepkov, I.V., et al., The Sytykanskaya kimberlite pipe: Evidence from deep-seated xenoliths and xenocrysts for the evolution of the mantle beneath Alakit, Yakutia, Russia, Geoscience Frontiers (2014), http://dx.doi.org/10.1016/j.gsf.2014.08.005

Table 3
Compositions of the minerals from the pyroxenite mantle xenoliths of Sytykan kimberlite pipe (Major elements are in in wt.% and trace elements in ppm).

Element	STk135 Gar pyroxnite			STk55 Gar pyroxenite		STk115 Gar websterite		STk9 Gar websterite		STk75 Gar websterite		STk60 Gar websterite		STk187 vein		STk196 vein		STk250 peridotite		
	Cpx	Gar	Phl	Cpx	Gar	Opx	Gar	Cpx	Gar	Cpx	Gar	Cpx	Gar	Cpx	Gar	Cpx	Gar	Cpx	Gar1	Gar2
SiO_2	55.1	41.34	42.14	55.09	41.79	58.64	41.85	55.47	41.2	56.03	42.38	54.78	42.53	56.23	41.63	54.54	42.43	55.68	41.9	41.6
TiO_2	0.05	0.10	0.21	0.22	0.17	0.04	0.03	0.04	0.09	0.12	0.24	0.25	0.21	0.16	0.21	0.08	0.25	0.30	0.17	0.15
Al_2O_3	0.772	19.87	11.93	2.7	22.76	0.503	20.66	0.802	19.88	1.03	21.95	3.38	21.83	1.95	21.42	1.34	21.99	4.96	21.14	22.14
Cr_2O_3	0.727	4.44	0.387	0.71	0.533	0.252	3.72	0.82	4.35	0.42	2.07	1.63	2.05	0.533	2.18	3.34	1.95	2.64	3.44	3.84
FeO	1.8	9.99	3.24	2.12	9.51	5.96	8.83	1.9	9.93	2.47	7.43	2.9	7.61	2.61	7.82	3.02	7.47	1.82	9.34	9.17
MnO	0.06	0.48	0.03	0.04	0.46	0.15	0.46	0.07	0.45	0.10	0.37	0.09	0.38	0.11	0.46	0.09	0.37	0.07	0.52	0.52
MgO	17.52	17.74	26.71	15.87	16.9	35.09	19.21	17.47	17.92	17.57	21.15	14.56	21.27	17.01	21.27	15.12	21.09	13.67	20.17	20.01
CaO	22.77	5.87	0.118	21.93	7.91	0.256	5.09	22.95	6.04	21.27	4.64	19.91	4.54	20.07	4.63	19.17	4.66	17.15	3.86	3.91
Na_2O	0.576	0.009	0.234	1.67	0.046	0.01	0.005	0.604	0.007	1.28	0.045	2.75	0.073	1.85	0.048	2.95	0.026	3.94	0.074	0.081
K_2O	0.017	0.01	9.57	0.01	0.01	0.006	0.004	0.018	0.01	0.024	0.01	0.01	0.005	0.022	0.004	0.011	0.009	0.015	0.011	0.12
Total	99.38	99.85	94.57	100.35	100.09	100.9	99.88	100.14	99.88	100.31	100.29	100.25	100.49	100.54	99.68	99.65	100.23	100.25	100.62	100.62
Ba	6.83	0.039	427	0.014	1.67	0.02	0.034	10.0	0.008	29.7	0.006	24.0	0.0	0.008	0.075	0.797	0.117	1.191	0.063	0.008
La	2.24	0.021	6.5	0.023	1.79	0.48	0.06	2.30	0.02	3.10	0.02	2.3	0.01	0.01	0.02	1.04	0.02	1.64	0.05	0.04
Ce	8.13	0.25	17.3	0.27	7.20	3.07	0.66	7.15	0.26	9.4	0.25	7.3	0.10	0.23	0.24	3.87	0.23	6.41	0.48	0.43
Pr	1.31	0.08	2.1	0.09	1.16	0.322	0.20	1.19	0.079	1.45	0.09	1.1	0.04	0.13	0.08	0.80	0.08	1.16	0.18	0.15
Nd	6.28	0.84	8.3	0.81	5.74	1.001	1.86	5.8	0.815	6.8	0.87	5.3	0.41	1.47	0.91	3.28	0.85	6.05	1.83	1.55
Sm	1.44	0.64	1.5	0.7	1.36	0.31	1.42	1.3	0.631	1.6	0.803	1.2	0.4	0.55	0.79	0.89	0.79	1.39	1.44	1.27
Eu	0.43	0.27	0.43	0.37	0.41	0.121	0.70	0.4	0.32	0.5	0.392	0.33	0.22	0.15	0.37	0.40	0.38	0.39	0.77	0.63
Gd	1.65	0.56	2.99	0.94	1.55	0.42	2.47	1.59	0.90	1.88	1.19	1.38	0.58	0.31	1.06	0.61	1.04	1.52	2.66	2.15
Tb	0.16	0.10	0.14	0.26	0.14	0.051	0.57	0.13	0.24	0.16	0.30	0.12	0.18	0.06	0.24	0.02	0.26	0.14	0.60	0.48
Dy	0.65	0.45	0.41	1.74	0.56	0.27	4.02	0.57	1.78	0.56	1.89	0.42	1.42	0.27	1.48	0.11	1.78	0.41	4.29	3.49
Ho	0.09	0.08	0.06	0.34	0.07	0.04	0.88	0.09	0.39	0.07	0.33	0.07	0.34	0.05	0.28	0.02	0.33	0.05	0.85	0.66
Er	0.26	0.25	0.19	0.94	0.21	0.10	2.53	0.22	1.17	0.18	0.95	0.15	1.15	0.14	0.82	0.03	0.97	0.15	2.35	1.76
Tm	0.02	0.05	0.01	0.13	0.02	0.02	0.34	0.02	0.17	0.01	0.12	0.01	0.18	0.02	0.12	0.003	0.15	0.01	0.29	0.22
Yb	0.10	0.39	0.07	0.89	0.08	0.16	2.18	0.10	1.26	0.07	0.88	0.06	1.22	0.18	0.90	0.01	1.08	0.04	1.98	1.38
Lu	0.013	0.07	0.01	0.14	0.01	0.04	0.31	0.01	0.20	0.01	0.15	0.01	0.21	0.04	0.15	0.00	0.19	0.01	0.28	0.21
Hf	0.65	0.62	0.28	1.04	0.57	0.14	2.16	0.57	1.1	0.56	1.34	0.42	0.72	0.42	1.11	0.20	1.19	0.46	2.37	1.98
Ta	0.02	0.02	0.33	0.02	0.01	0.02	0.04	0.07	0.02	0.11	0.02	0.067	0.009	0.002	0.02	0.007	0.02	0.02	0.054	0.038
Pb	0.17	0.007	0.31	0.01	0.17	0.01	0.01	0.14	0.01	0.29	0.01	0.184	0.005	0.003	0.013	1.66	0.01	0.13	0.009	0.007
Th	0.071	0.004	0.36	0.007	0.02	0.052	0.012	0.09	0.007	0.15	0.004	0.102	0.002	0.003	0.005	0.022	0.005	0.02	0.012	0.009
U	0.016	0.008	0.09	0.014	0.004	0.055	0.023	0.021	0.009	0.033	0.01	0.014	0.004	0.005	0.01	0.01	0.011	0.004	0.021	0.036
Co	23.6	36.9	29.7	31.7	20.1	25.9	38.5	16.8	30.1	17.9	30.1	14.6	20.6	22.5	26.2	60.7	23.4	15.2	26.3	27.2
Cu	1.87	0.49	3.17	0.50	1.95	0.11	0.78	1.33	0.42	2.64	0.26	0.78	0.10	0.01	0.25	3.79	0.17	0.89	0.29	0.28
Ni	334	96	630	75	478	32	122	345	91	432	72	319	39	20	60	1831	54	374	69	70
Rb	0.35	0.007	6.5	0.012	0.015	0.011	0.013	0.62	0.091	3.26	0.011	7.02	0.0005	0.008	0.009	0.39	0.01	0.07	0.01	0.01
Sr	113	0.3	157	0.3	111	4.3	1.2	104.4	0.3	165	0.3	131	0.2	0.3	0.5	65.6	0.3	120	0.6	0.5
Y	2.0	2.06	1.48	8.69	1.70	1.2	20.8	1.9	9.9	1.6	8.9	1.3	8.6	1.2	7.2	0.0	8.6	1.2	20.3	15.8
Zr	8.4	26.7	9.3	46.1	7.0	9.6	76.5	7.5	37.9	8.4	54.0	6.3	27.9	12.3	45.0	2.7	47.9	6.1	94.0	0
Nb	0.63	0.48	3.41	0.58	0.24	0.74	0.91	0.98	0.35	1.48	0.46	1.18	0.18	0.38	0.52	0.14	0.46	0.29	0.81	0.76

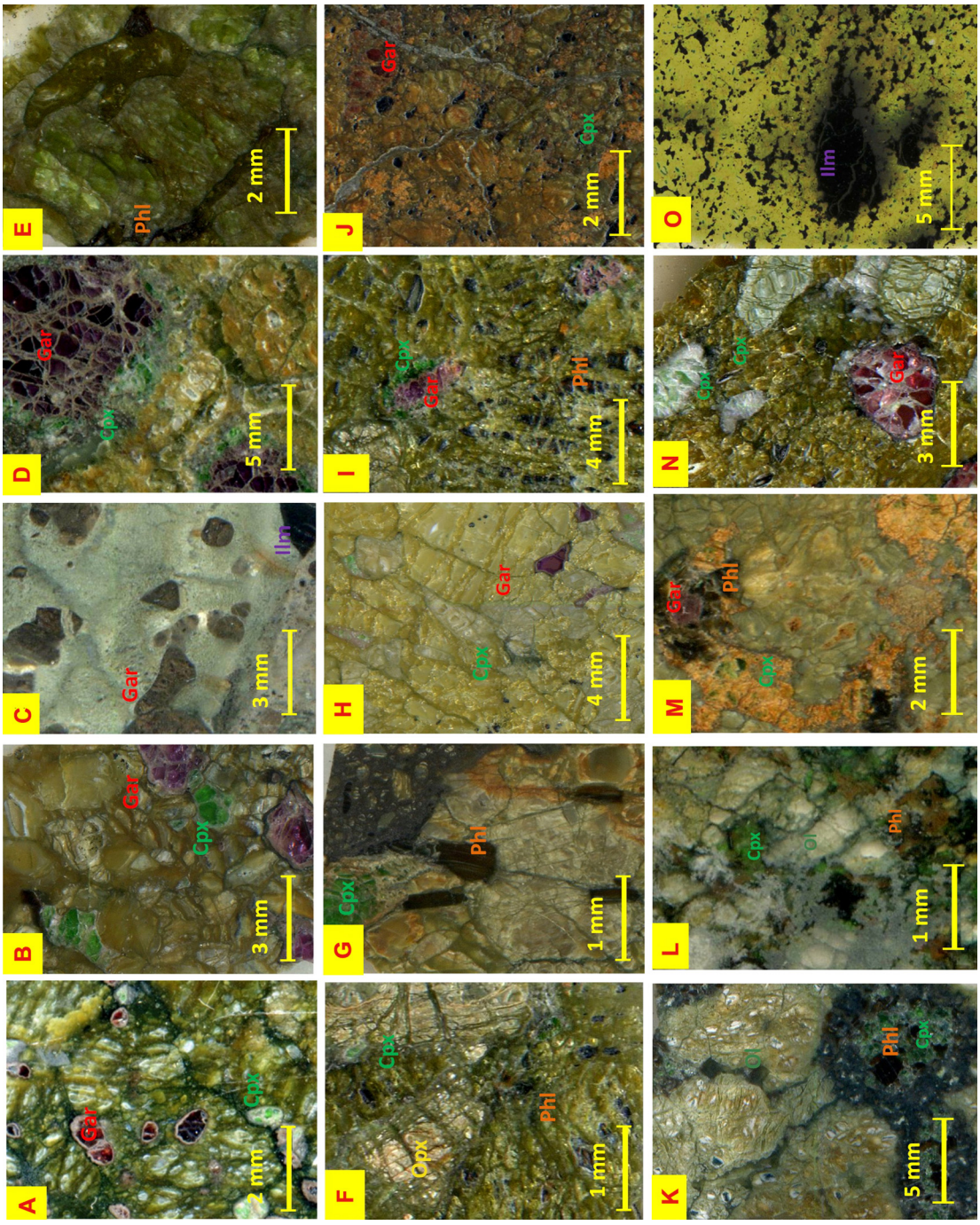

Figure 2. Photo images of the mantle xenoliths from Sytykanskaya pipe. (A) Fine grained granular garnet lherzolite; (B) Coarse grained granular garnet lherzolite; (C) Deformed garnet peridotite; (D) Details of garnet lherzolites: Cpx corona on garnet; (E) Ilmenite bearing peridotite; (F) Sp – harzburgite; (G) Garnet harzburgite with the disseminated idiomorphic phlogopite; (H) Garnet dunite; (I) Garnet harzburgite with the Phl; (J) Serpentinized garnet bearing harzburgite with abundant intergranular Ilmenite; (K) Details of substitution of garnet grains by Cpx-Phl-Ilm aggregates; (L) Phl-Cpx-Ulvospinel-Ilm veinlets in peridotites; (M) Garnet harzburgite with the garnet partly substituted by Phl and Cpx; (N) Garnet harzburgite with disseminated Ilm and Phl; (O) Deformed ilmenite peridotite.

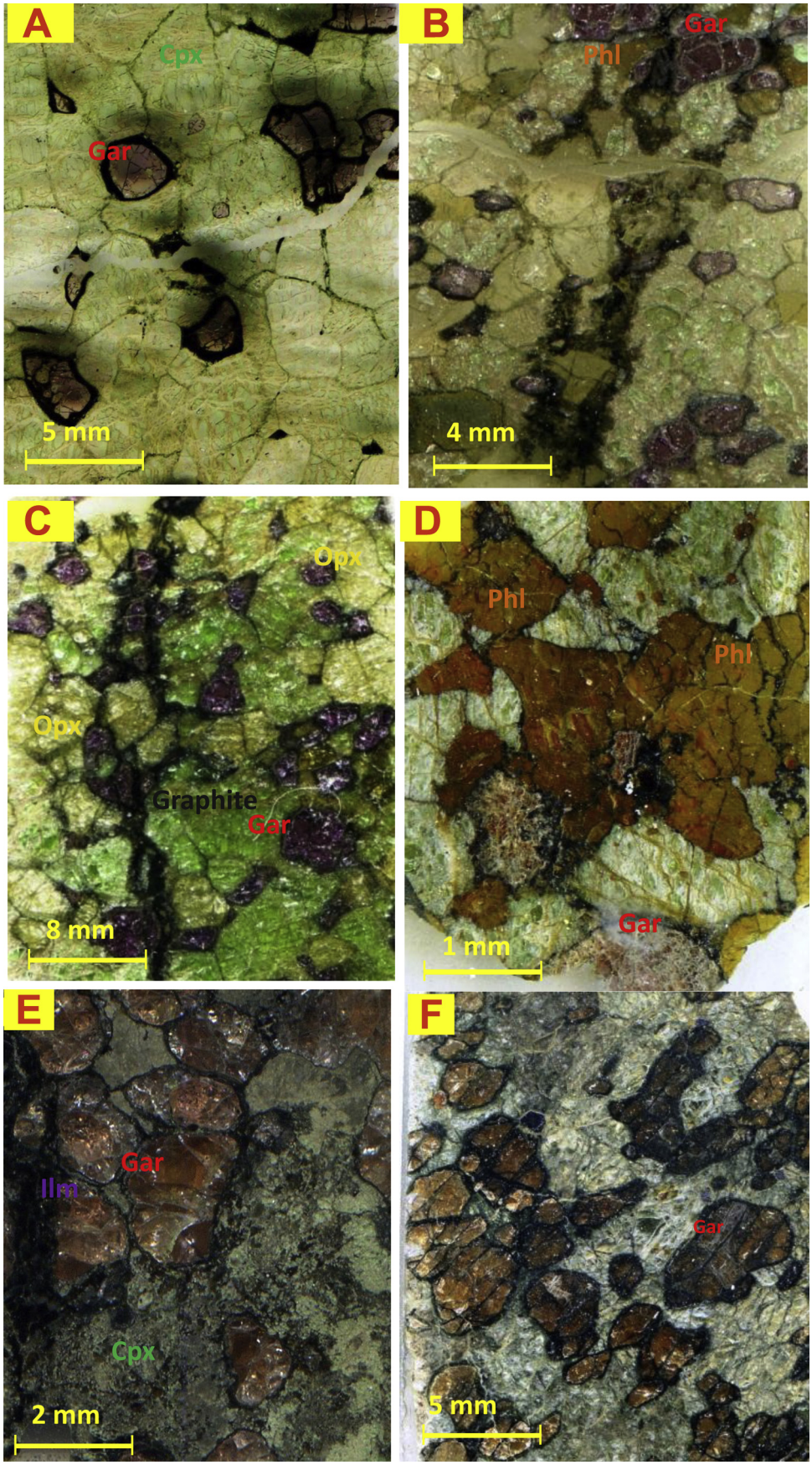

Figure 3. Images of scanned thin sections of pyroxenite and eclogite mantle xenoliths. (A) Garnet Cr-bearing webstrite; (B) Gar Cr-diopside websterite with Phl vein; (C) Cr-diopside websterite with graphite; (D) Phlogopite, ulvospinel, ilmenite in Ilmenite-bearing peridotite with Cr-diopside and relics of garnets; (E) Bi-mineral eclogite; (F) Eclogite with the relics of Cpx and intergranular reaction products.

Please cite this article in press as: Ashchepkov, I.V., et al., The Sytykanskaya kimberlite pipe: Evidence from deep-seated xenoliths and xenocrysts for the evolution of the mantle beneath Alakit, Yakutia, Russia, Geoscience Frontiers (2014), http://dx.doi.org/10.1016/j.gsf.2014.08.005

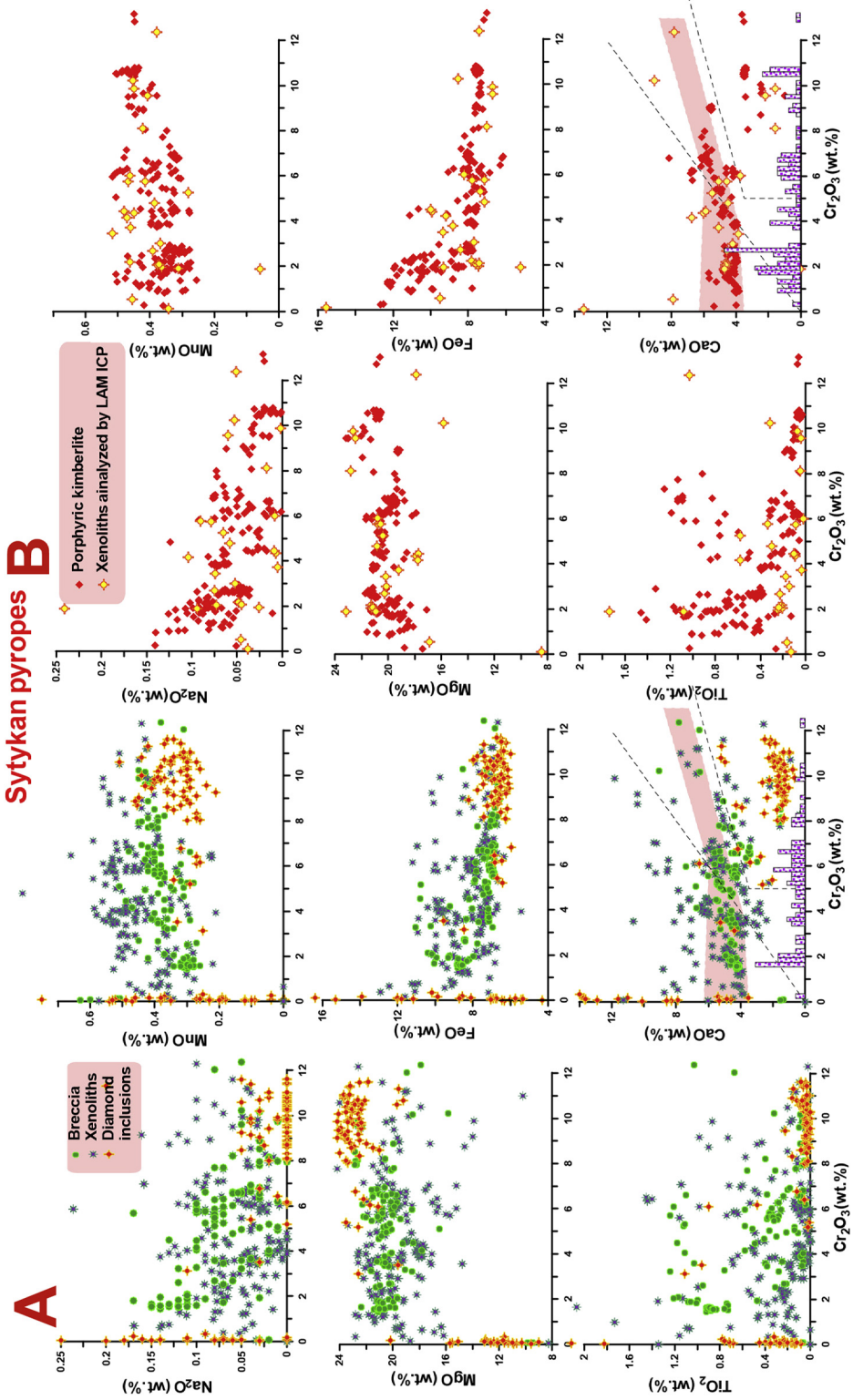

Figure 4. Compositions of the pyropes (A) from breccia and (B) porphyric kimberlites from Sytykanskaya pipe. In addition in (Fig. 1A) the compositions of the garnets from analyzed xenoliths and diamond inclusions are shown. And in Fig. 1B compositions of the garnets from veined metasomatites and pyroxenites analyzed by LAM-ICPMS. The fields in Cr_2O_3-CaO diagram are after Sobolev et al. (1973).

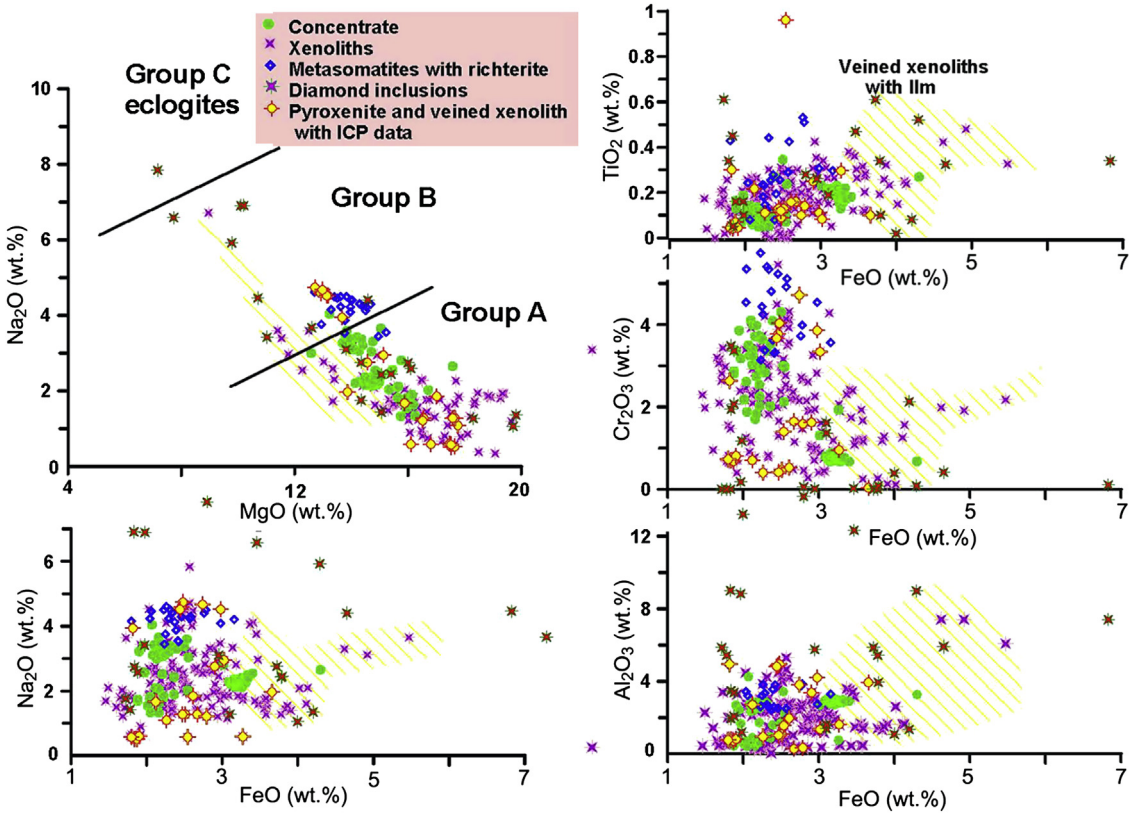

Figure 5. Compositions of Cr-diopsides from breccia and porphyric kimberlites from Sytykanskaya pipe. Dashed field is for the associations with ilmenites.

Kostrovitsky et al., 2006) but the Cr content in general is much lower than in Sytykanskaya and other Alakit pipes. The trend of ~0.5 is parallel to the TiO_2 axe and formed by the fraction of uncontaminated protokimberlite melts. There is abrupt linear increase in this component from 2 to 3 wt.% in the middle part of the TiO_2 trend. A further two levels ~3.5 and 5 wt.% Cr_2O_3 in the middle part of the TiO_2-Cr_2O_3 trends belong to the phlogopite-bearing metasomatites and glimmerite with alkali amphiboles which have very high Cr contents. In the left low-Ti part of the trend, there are several levels of the Cr-enrichment also.

The ilmenite trend from the ABK and xenoliths (Fig. 7A) are nearly coinciding and reveal division into the same clusters and trends with the boundaries referring to the close levels but the trends are more dispersed. Mg-rich low-Cr (group 1) ilmenites from Sytykanskaya pipe which are also found in some Ilm dunites show Cr decreases together with the TiO_2. The MnO content is also decreasing in general. The Cpx-bearing Ilm rocks are commonly higher in Cr. But those with Phl are more Cr-enriched. The ilmenites with low TiO_2 and MgO are relatively rare among the xenoliths.

Amphiboles in the Sytykanskaya pipe were found in the veins with phlogopites and ilmenites. Only those found in alkaline glimmerites are close to richterites (Hawthorne and Oberti, 2007). Since they are not so high pressure as those obtained in the high pressure experiments at 7.0–9.0 GPa (Konzett and Ulmer, 1999), they are the K-Na type which was obtained in experiments at 3–4 GPa (Sweeney et al., 1993). Similar amphiboles were found in the harzburgites from Udachnaya pipe (Solov'eva et al., 1997). Amphiboles from Sytykanskaya xenoliths are more Cr-rich comparing with the richterites from MARIDs (Dawson and Smith, 1977, 1982; Boyd, 1990; Konzett et al., 2000, 2013) but are close to those in South Africa kimberlites (Dawson and Smith, 1982; Gregoire et al., 2002, 2003). Most amphiboles from veined xenoliths from Sytykanskaya are Cr-pargasite and one is pargasitic hornblende, similar to those found in the northern parts of Yakutia (Ashchepkov et al., 2004). The silica content for amphiboles is correlating with the pressures (Niida and Green, 1999). Only one pargasite from the ilmenite-bearing vein reveals high Ti content (Fig. 8).

Phlogopites from Sytykanskaya xenoliths are highly variable in composition (Fig. 9). For the low-Fe varieties two levels of the Cr_2O_3 enrichment are visible: 0.5 and 2 wt.% Cr_2O_3. Phlogopites with FeO >4 wt.% and Cr_2O_3 close to 4–5 wt.% are from the ilmenite-bearing veins. The Na_2O content is also up to 0.8 wt.% being lower in the middle part of the trend and high for the ilmenite-bearing associations. In the middle part of the diagram the TiO_2 level is highest ~2–5 wt.%. Variations with increasing admixtures in phlogopites are accompanied by a decrease in SiO_2. The rise of Ti, Na, and Cr corresponds to the increase of the Al/(Al + Si) or eastonite component which corresponds to a pressure decrease (Arai, 1984; Mitchell, 1995).

5. PTX diagrams and variation of the oxygen fugacity conditions

For the calculations of the P-T-$f(O_2)$ conditions we used combinations of the common thermobarometric methods (Brey and Kohler, 1990; Nimis and Taylor, 2000) and monomineral methods for garnets (Gar), clinopyroxenes (Cpx), chromites (Chr) and ilmenites (Ilm) (Ashchepkov et al., 2010, 2012, 2013a,b) realized in the slightly modified PT program (see Supplement File 2). The thermobarometers for Cpx and Gar were checked using experimental data sets for peridotite (950°C) and eclogite systems (530°C). New introductions were introduced into Gar, Chr and Ilm barometers to increase the agreement between the calculated PT values with the experimental conditions (Ashchepkov et al., 2011).

Please cite this article in press as: Ashchepkov, I.V., et al., The Sytykanskaya kimberlite pipe: Evidence from deep-seated xenoliths and xenocrysts for the evolution of the mantle beneath Alakit, Yakutia, Russia, Geoscience Frontiers (2014), http://dx.doi.org/10.1016/j.gsf.2014.08.005

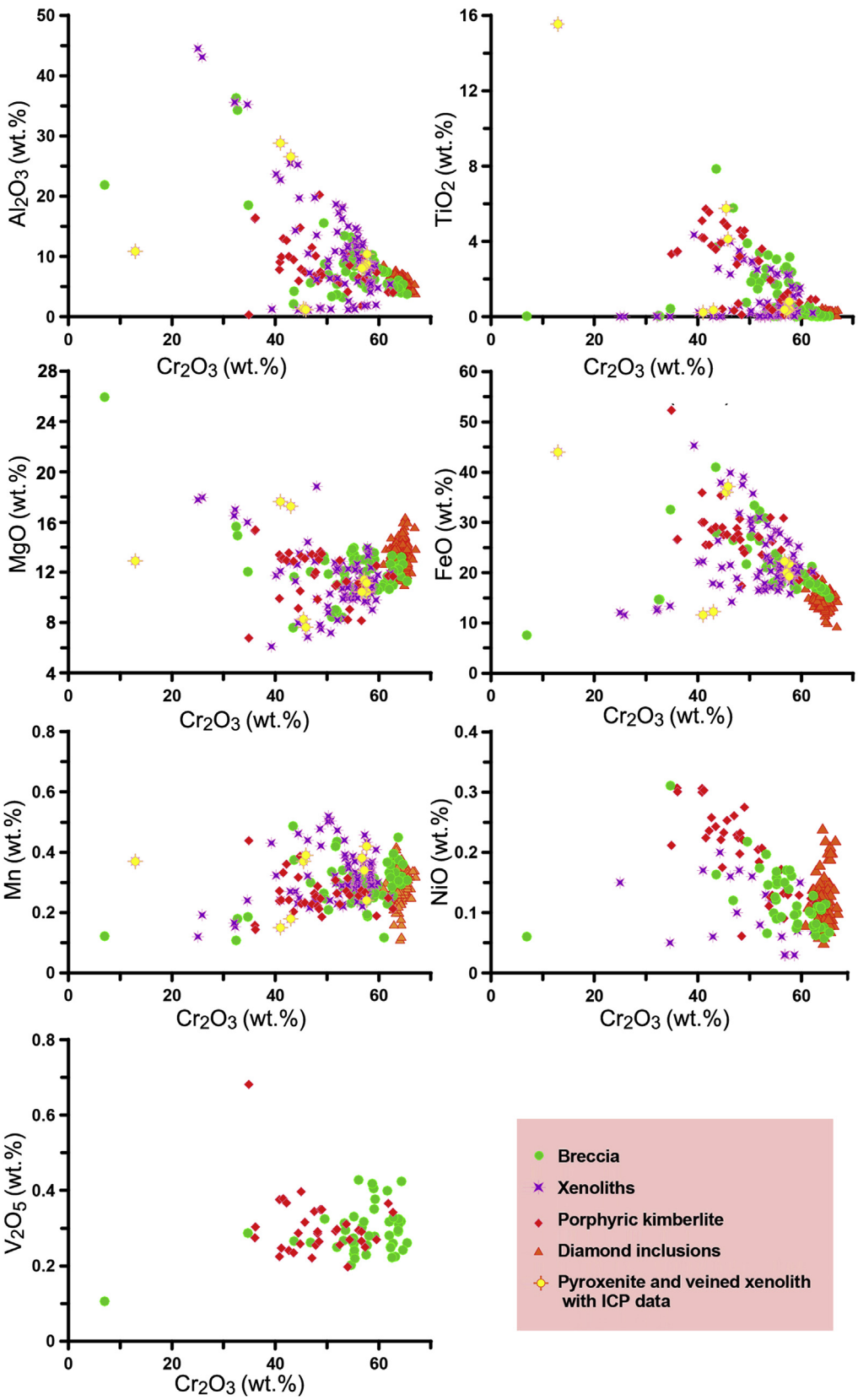

Figure 6. Compositions of chromites from breccia and porphyric kimberlites from Sytykanskaya pipe.

Please cite this article in press as: Ashchepkov, I.V., et al., The Sytykanskaya kimberlite pipe: Evidence from deep-seated xenoliths and xenocrysts for the evolution of the mantle beneath Alakit, Yakutia, Russia, Geoscience Frontiers (2014), http://dx.doi.org/10.1016/j.gsf.2014.08.005

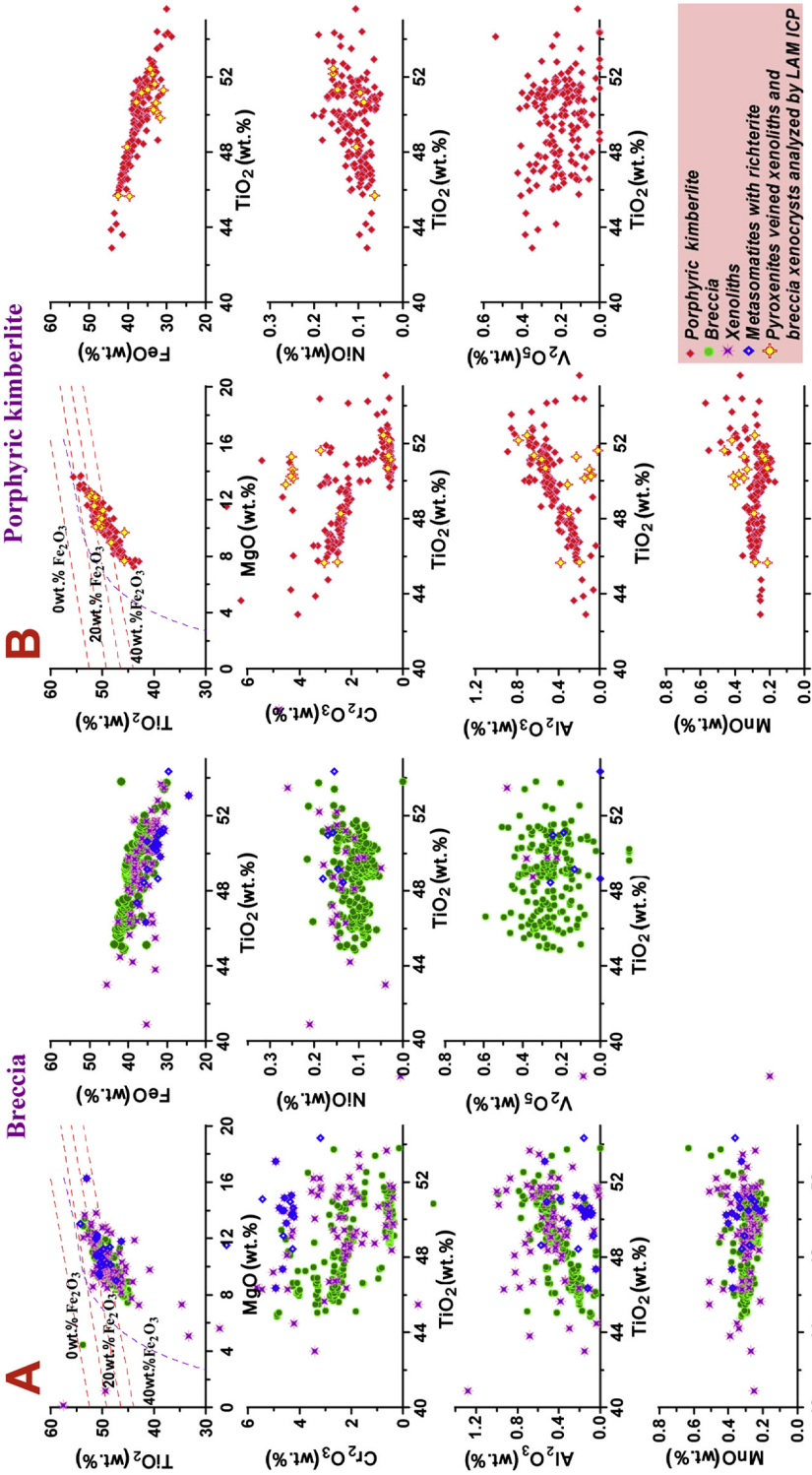

Figure 7. Compositions of ilmenites from breccia (A) and porphyric kimberlites (B) from Sytykanskaya pipe.

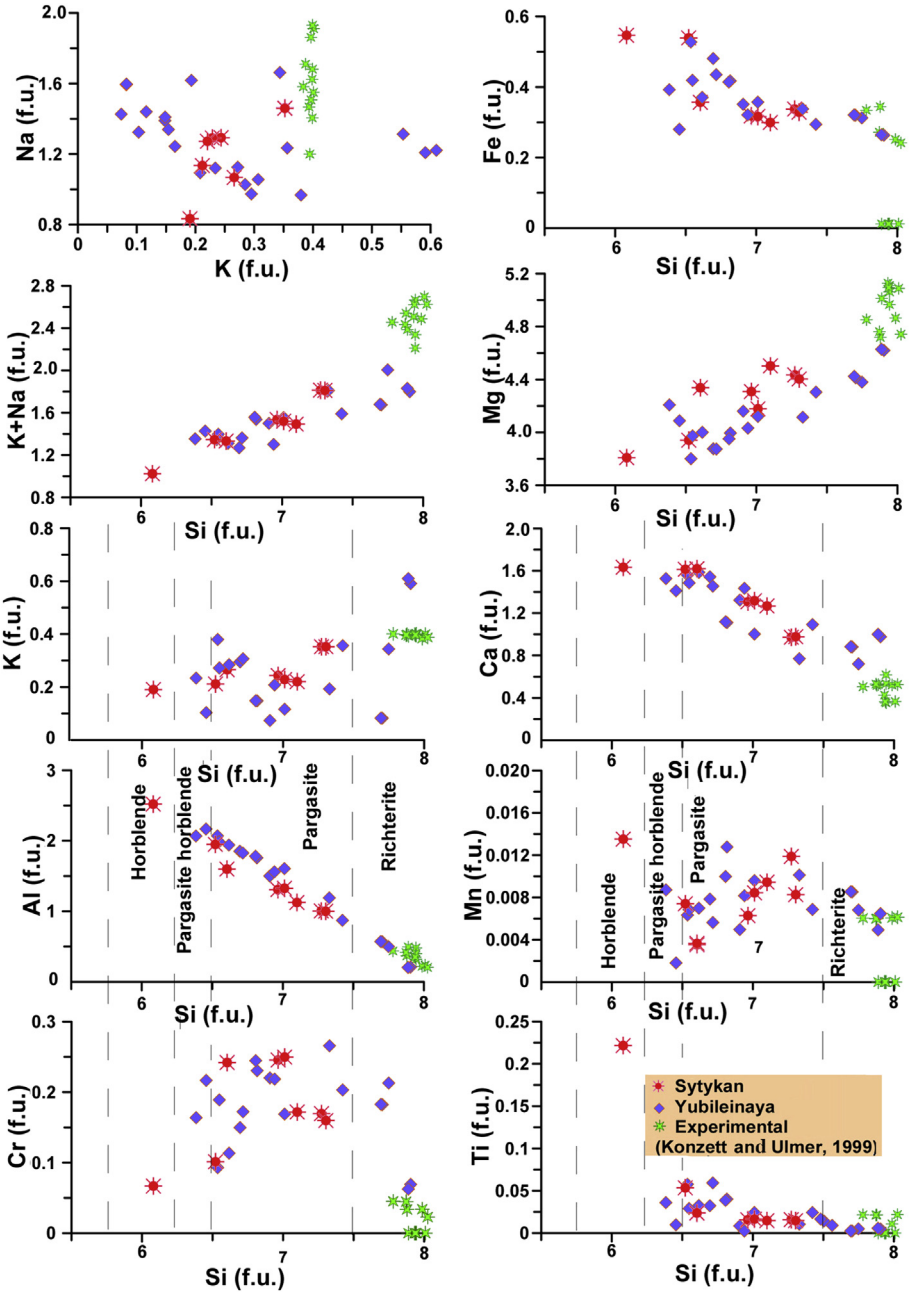

Figure 8. Compositions of amphiboles from breccia and mantle xenoliths from Sytykanskaya pipe in comparison with those from concentrate of Yubileynaya pipe (Ashchepkov et al., 2004, 2010) and experimental data from the MARIDS (Konzett and Ulmer, 1999).

P-T conditions for garnet xenocrysts from porphyric kimberlites (Fig. 10A) create nearly linear trends close to 600 °C at the Moho and descending to 35 mW/m^2 geotherm at 6.5 GPa where there is an inflection corresponding to the convective branch, determined in many mantle sections (Boyd, 1973; Rudnick et al., 1998; Kopylova et al., 1999). Similar geotherm is calculated by the Gar-Opx thermobarometry (Brey and Kohler, 1990) (Fig. 11). The convective branch is marked by the high temperature (HT) trends for ilmenites and diamond inclusions of chromites and garnets. The pronounced inflection of ilmenites, diamond inclusions of eclogitic Cpx and Garnets is determined at 3.5–4 GPa along the graphite–diamond transition line (Kennedy and Kennedy, 1976) which is corrected to the lower pressures (Day, 2012). This explains position of the essential amount of diamond inclusions above the diamond stability field. The double geothermal arrays are detected between 4 and 6 GPa which probably is correspondent to the influence of protokimberlite system created picroilmenites. Such geothermal trends with a deviation from the conductive geotherms in the upper part were determined in the continental mantle of many regions worldwide (Dawson, 1980; Boyd et al., 1997; Rudnick et al., 1998; Batumike et al., 2009; Ashchepkov et al., 2013a,b,c). Eclogitic Cpx from the diamond inclusions (DI) (Efimova and Sobolev, 1977; Sobolev et al., 2004; Logvinova et al., 2005; Logvinova and Ashchepkov, 2008; Spetsius and Koptil, 2008) shows wide range of geothermal conditions in middle and lower part of the mantle section. The Opx inclusions together with Gar refer to the most low temperature (LT) cluster near 3.5 GPa, which is common for the other mantle sections (Ashchepkov et al., 2013a). Chromite

Please cite this article in press as: Ashchepkov, I.V., et al., The Sytykanskaya kimberlite pipe: Evidence from deep-seated xenoliths and xenocrysts for the evolution of the mantle beneath Alakit, Yakutia, Russia, Geoscience Frontiers (2014), http://dx.doi.org/10.1016/j.gsf.2014.08.005

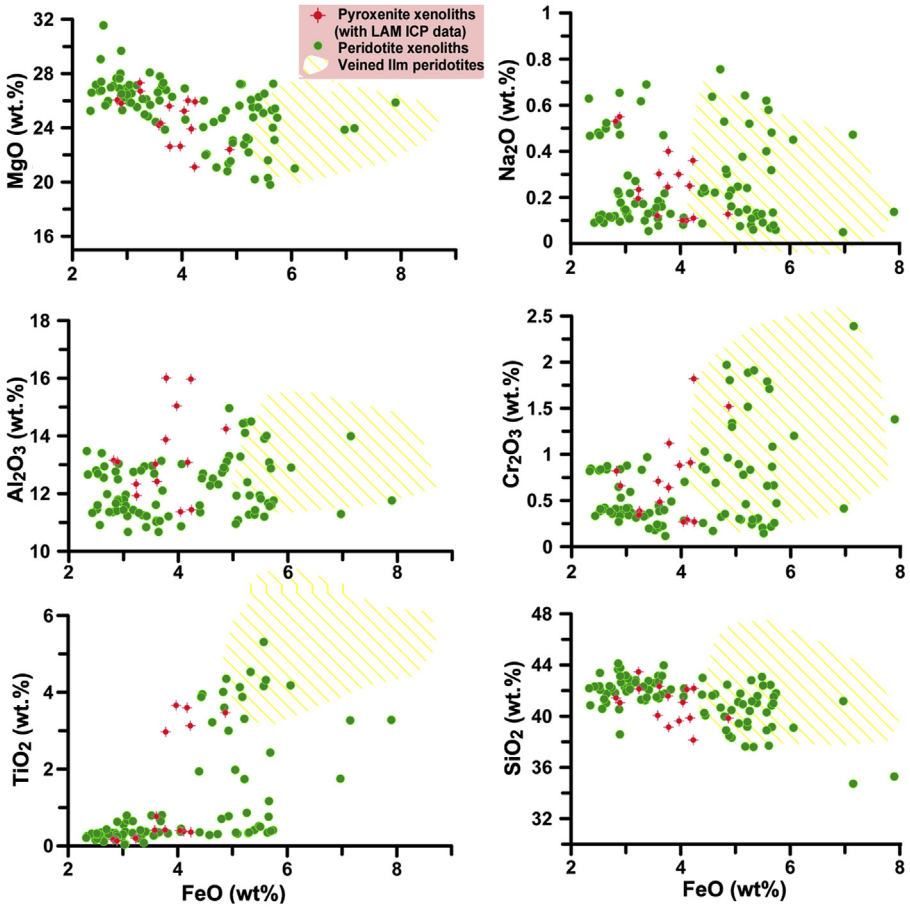

Figure 9. Compositions of phlogopites from breccia and mantle xenoliths from Sytykanskaya pipe.

diamond inclusions represent the compact cloud deviated to the HT part of the diagram for deformed garnet peridotite and ilmenite megacrysts at 7–5.5 GPa interval. The Cpx diamond inclusions mostly trace the diamond–graphite line from the most LT conditions for the Cr-low varieties to HT branch for the eclogites of Cr bearing hybrid type.

In this interval the Fe-content of garnets is rising from the lithosphere base in 6 intervals from 7.5 to 1.5 GPa and rapidly rise from 2.5 GPa. The PT estimates for chromite and ilmenite coincide in pressure, but chromites mark relatively lower temperature conditions and reveal lower $Fe^{\#}$ but mostly higher than garnets. Probably the formation of this mineral occurs at the outer contacts of the protokimberlite feeders and in metasomatic veins.

Kinks in P-$Fe^{\#}$ are observed near 3.2, 2.8 and 1.6 GPa. At the bottom of the chart, which presents the PTX estimates for inclusions in diamonds, there are 4 pressure intervals where CaO content in garnets is rather stable. The CaO content in garnets is fluctuating in certain pressure intervals and abruptly split near 4.5 and 5.0 GPa. Very high Cao is typical for the pyroxenites and some eclogites from the middle pyroxenite lens (Pokhilenko et al., 1999) which is detected in most mantle sections in Daldyn and Alakit fields (Ashchepkov et al., 2010, 2013a).

The ilmenite P-$f(O_2)$ trend of Sytykanskaya reveals comparatively oxidized conditions in the lithosphere base and then became less oxidized, unlike other mantle sections in Yakutia (Ashchepkov et al., 2004, 2013a,b,c), where it usually traces the dividing line of the stability of carbonatite melt and diamond (Stagno and Frost, 2010; Stagno et al., 2013) which is close to the diamond stability field found by McCommon et al. (2001). The variations of oxidizing conditions defined for garnet and chromite are limited by this line on the left. Above 4.0 GPa oxidizing conditions for all minerals increase drastically.

For the xenocrysts found in ABK the general variations of the P-$Fe^{\#}$ trends are similar. However, the diversity of linear and curved skew trend appears to be higher, probably due to the influence of several branched systems of melts derived from kimberlites in different levels.

Actually picroilmenites formed by protokimberlite melt (Dowson et al., 1982; More and Lock, 2001; Ashchepkov et al., 2010) formed two large clusters in mantle column. The ilmenites and their parental melts in the lithosphere base are low in Cr_2O_3 and become significantly enriched in Cr_2O_3 near 4.5–3.5 GPa. The CaO and FeO trends for garnet at each level have formed separate trends which are similar to those from PK but are more dispersed.

Clinopyroxenes from the breccia reveal mostly low pressure conditions. Deviations to HT conditions for Cr-bearing Cpx from peridotites occurs at several levels, ranging from 6.5 to 3.5 GPa, which corresponds also to the metasomatites marked mainly by ilmenite PT points. Clinopyroxenes with $Fe^{\#}Ol$ ($\sim$15%) are close in $Fe^{\#}$ to the most Fe-rich varieties of ilmenites which were formed from the latest and most fractionated derivatives of protokimberlite systems that after the crystallization of ilmenite-diopside systems created significant amounts of diopside-phlogopite veins at the top of the mantle section. Associations with ($Fe^{\#}Ol = \sim 11–12$) were formed by another more magnesian system that created polymineral Cpx-Gar-Ilm associations.

The arrays on the P-$f(O_2)$ diagrams look more stable in separate pressure intervals. For the chromite oxidation stage variations are

Please cite this article in press as: Ashchepkov, I.V., et al., The Sytykanskaya kimberlite pipe: Evidence from deep-seated xenoliths and xenocrysts for the evolution of the mantle beneath Alakit, Yakutia, Russia, Geoscience Frontiers (2014), http://dx.doi.org/10.1016/j.gsf.2014.08.005

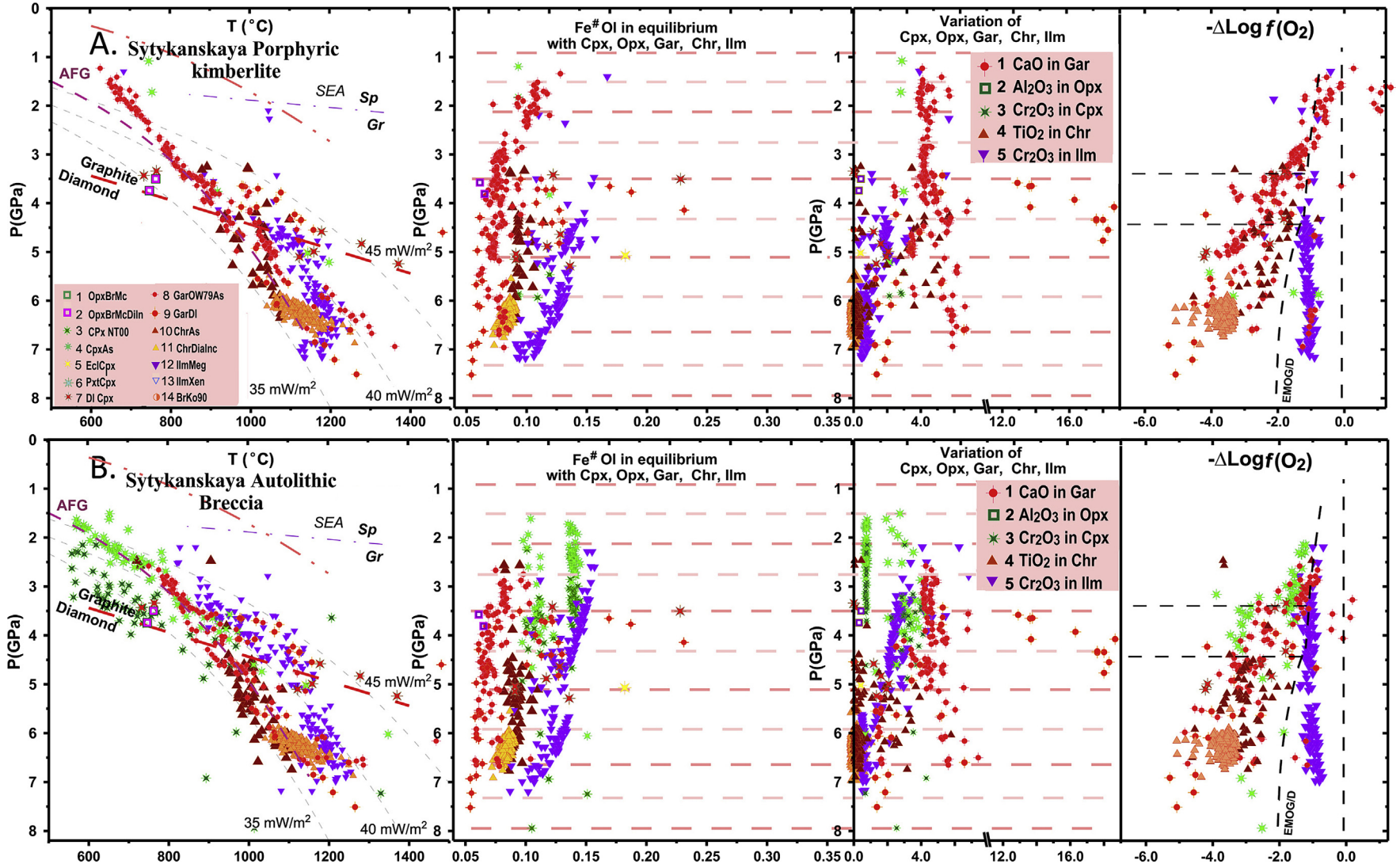

Figure 10. (A) P-T-X-$f(O_2)$ diagram for the concentrate from porphyric kimberlite from Sytykanskaya pipe and diamond inclusions according to Spetsius and Koptil (2008). Signs: Opx: 1. T(°C) (Brey and Kohler, 1990)-P(GPa) (McGregor, 1974); 2. The same for diamond inclusions. Cpx: 3. T(°C)-P(GPa) (Nimis and Taylor, 2000); 4. T(°C) (modified from Nimis and Taylor, 2000)-P(GPa) (Ashchepkov et al., 2010); 5. The same for eclogites; 6. The same for pyroxenites; 7. The same for diamond inclusions. Garnet (monomineral): 8. T(°C) (O'Neill and Wood, 1979)-P(GPa) (Ashchepkov et al., 2010); 9. The same for diamond inclusions. Chromite: 10. T(°C) (O'Neill and Wall, 1987)-P(GPa) (Ashchepkov et al., 2010); 11. The same for diamond inclusions. Ilmenite megacrysts: 12. T(°C) (Taylor et al., 1998)-P(GPa) (Ashchepkov et al., 2010); 13. The same for xenoliths; 14. T(°C)-P(GPa) (Brey and Kohler, 1990). The compositions of the diamond inclusions are taken from Sobolev et al. (2003, 2004) and Logvinova et al. (2005). The field for the diamond bearing associations after Stagno et al. (2013). The horizontal dashed line at 3.5 and 4.5 GPa corresponds to the Graphite–Diamond boundary at 35 and 40 mW/m^2 respectively. (B) P-T-X-$f(O_2)$ diagram for the concentrate from autolithic breccia from Sytykanskaya pipe and diamond inclusions according to Spetsius and Koptil (2008). Signs are the same as in Fig. 11.

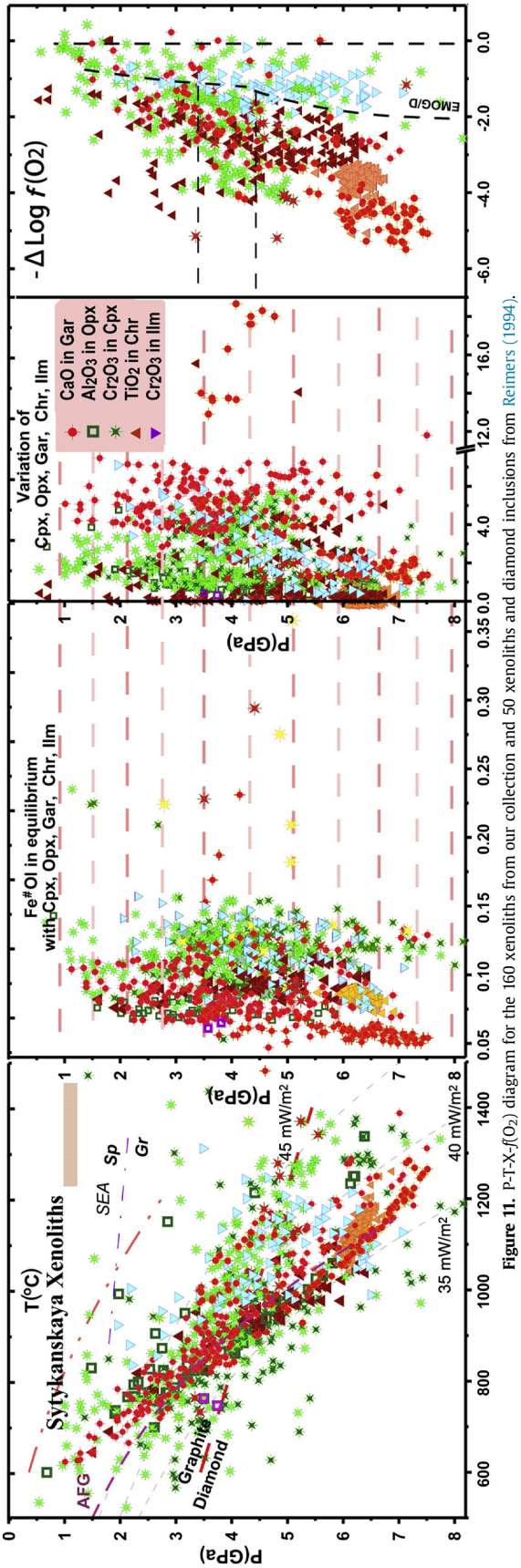

Figure 11. P-T-X-$f(O_2)$ diagram for the 160 xenoliths from our collection and 50 xenoliths and diamond inclusions from Reimers (1994).

similar to those from the porphyritic kimberlites but the amount of chromites in the deepest levels is higher.

PTX diagrams for the xenoliths (Fig. 11) show a different configuration of trends and clusters in P-Fe#, X diagrams for some minerals, reflecting variations of peridotite associations. PT conditions for the most commonly used thermobarometry for 10 associations (Brey and Kohller, 1990) nearly repeat the garnet geotherm from 6.5 to 2.0 GPa. This is the first polymineral geotherm for the mantle in the Alakit field. The PT estimates based on clinopyroxenes (Nimis and Taylor, 2000; Ashchepkov et al., 2010, 2012, 2013a,b) give somewhat similar but broader range, reflecting high-temperature and low-temperature branches. The combined geotherms give step deviation to 35 mW/m^2 conductive branch similar to those for mantle beneath Udachnaya (Boyd et al., 1997; Ashchepkov et al., 2010, 2013a,b; Ionov et al., 2010; Doucet et al., 2012; Goncharov et al., 2012). Clinopyroxene geotherms for Sytykanskaya are similar to those determined beneath the Daldyn field, and quite different from those determined for the mantle beneath Yubileynaya pipe (Ashchepkov et al., 2004).

The high pressure part of the ilmenite trend is formed by the uncontaminated low-Cr varieties but in the upper part the Cr-content increases. However, at the level of 4.0 GPa, it is growing abruptly.

Some variations in the high-temperature part of the diagram near ~3.5 and 4.0 GPa corresponds to the metasomatites, thus marking the positions of the fluid-saturated melts like on South Africa (Gregoir et al., 2002, 2003; Gibson et al., 2008; Lazarov et al., 2012). The highest temperature conditions are defined by orthopyroxenes and ilmenites and clinopyroxene diamond inclusions which could be formed from protokimberlite derivatives.

Almost linear trends of Fe# for the pyroxenes of chromite in the middle part of the mantle columns correspond to the three types of evolving magmatic system responsible for the existence of at least three separate types of metasomatites. Most ferrous 0.14–0.15 Fe# was for the Cpx and Ilm at depths of 5.5–6.5 GPa and slightly above which is correspondent to the Ilm peridotites. Two varieties with Fe#Ol (11 and 12.5%) were generated within the 5.5 to 3.7 GPa interval.

Two Gar-Cpx-Ilm sub-trends in Fe#Ol (~6–9%) show the primary layering in the mantle. In the lower part of the mantle column, mantle inclusions create an evolving Fe-trend from the garnets to chromite diamond inclusions. Variation of CaO for the garnets from xenoliths is higher than for xenocrysts. Variations of Cr-clinopyroxene of the xenoliths are also higher and vary in each level of the mantle column.

Very wide variations of oxidizing conditions are characteristic for the pyroxenes and garnets from xenoliths in each level of the P-$f(O_2)$ for xenoliths which may correspond to the intrusions of the different melt portions and metasomatic gradients near the contacts. The widest variations of P-Fe#, $f(O_2)$ are defined near the pyroxenite lens (Pokhilenko et al., 1999). Veins with phlogopite, ilmenites and alkaline amphiboles close to richterites were formed there as well as websterites with graphite and phlogopite. The most Fe#Ol rich metasomatic clinopyroxenes, ilmenite and phlogopites occur in the middle part of the section. The most Cr-rich varieties are located at 3.0 GPa.

6. Variations of trace elements of xenocrysts and xenolith minerals

Rare earth element patterns were analyzed for three types of samples including xenocrysts from the breccia, metasomatic xenoliths, and glimmerites xenolith with alkaline amphiboles and garnet websterites with graphite.

There are systematic variations for TRE in each group. For Cr-diopsides from the breccia (Fig. 12A) there are two major types of

Please cite this article in press as: Ashchepkov, I.V., et al., The Sytykanskaya kimberlite pipe: Evidence from deep-seated xenoliths and xenocrysts for the evolution of the mantle beneath Alakit, Yakutia, Russia, Geoscience Frontiers (2014), http://dx.doi.org/10.1016/j.gsf.2014.08.005

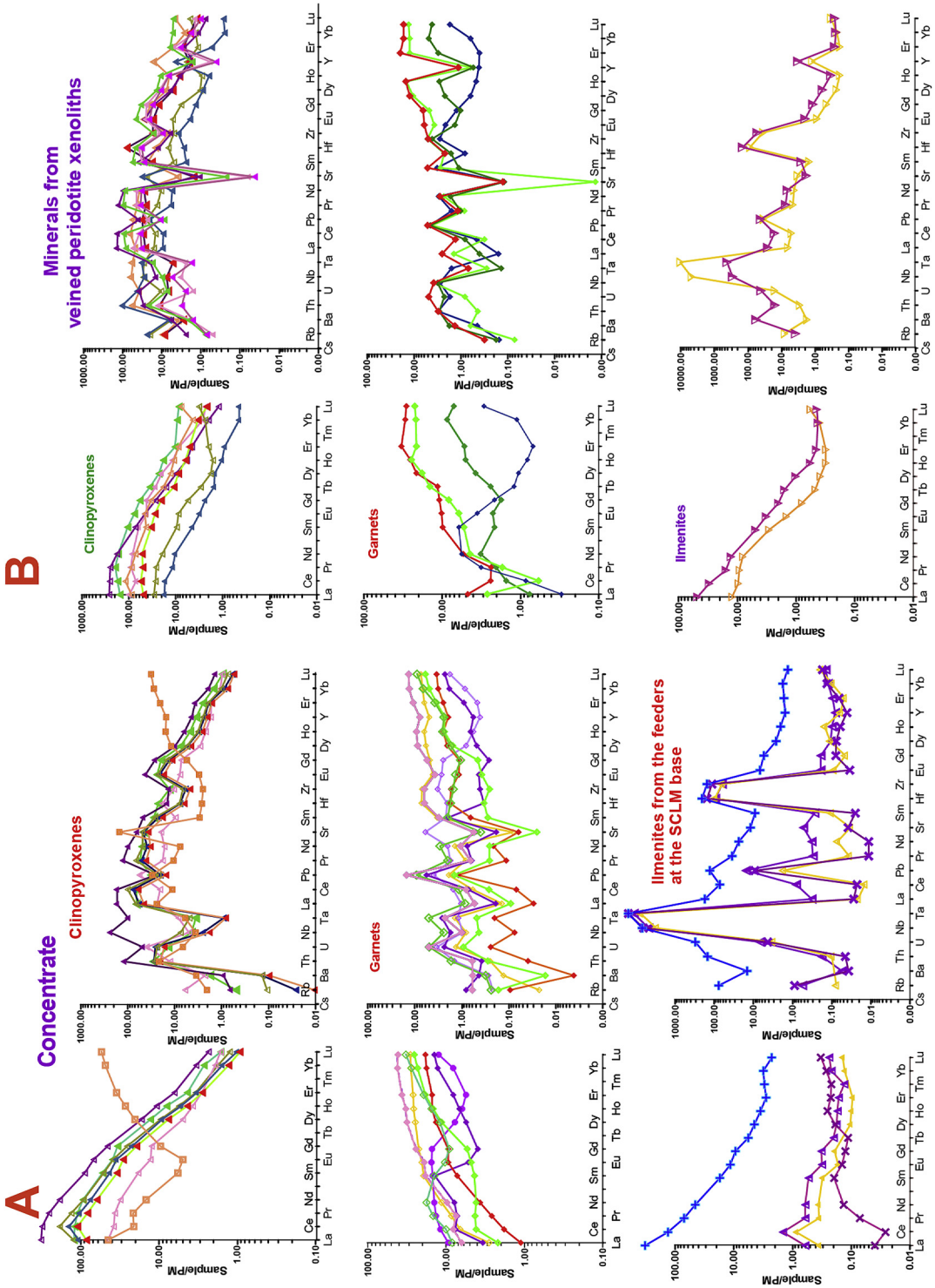

Figure 12. (A) REE and TRE spider diagrams for the minerals from concentrates breccia of Sytykanskaya pipe. Dashed lines are for the range of kimberlite compositions. (B) REE patterns and TRE spider diagrams for the minerals from metasomatic xenoliths of Sytykanskaya pipe. Normalization to primitive mantle after McDonough and Sun (1995).

spectrums. The samples with the highest $(La/Yb)_n$ (~400) ratios and $(La/Ce)_n$ ~1 corresponds to the relatively low pressures. While the other with $(La/Yb)_n$ (45–10) ratios high $(La/Ce)_n$ and less inclined and nearly lineal spectrums are more deep seated. These two types of Cpx patterns both show rather deep Ta, Nb and smaller Zr troughs. The most enriched Cpx spectrum has La ~500 higher than values of primitive mantle and reveals no minimum of high field strength (HFSE) and elevated Ba, U. One Cpx spectra with the V type spectrum is close to depleted Gar-free harzburgites of front- or back-arc (Ionov et al., 2013).

Garnets reveal also flattened REE distributions without essential HFSE and as usual are dominated by the HREE. Some garnets have S-shaped spectra. But sharp dips in Sr and high Pb, U peaks which are common for some lithospheric mantle peridotite (Ionov et al., 2010; Doucet et al., 2012) were not found. They reveal elevated Th, U contents and even Ta, Nb and some as well Zr-Hf.

There are two types of ilmenite REE patterns. The first one shows flattened patterns, typical for the most Mg-rich ilmenites (Clarke and Mackay, 1990.). The other type reveals highly inclined patterns, enriched in LREE. All of them have HFSE maxima and are enrichment in Y which increases along with the level of REE.

Clinopyroxenes from the metasomatic peridotites (Fig. 12B) are also characterized by the slightly lower inclination of REE patterns and $(La/Ce)_n$ and $(La/Pr)_n$ <1 as a rule. This means that the melting degrees for the parental melts are higher than for the previous group, and the Gar/Cpx ratios in the rocks are lower. The level of depletion of the Zr is quite high. For many of the analyzed garnets, especially from the deep part of the mantle column, the deep troughs of MREE or S-spectra are found.

Ilmenites from xenoliths are characterized by inclined REE patterns and HFSE peaks slightly lower than the ilmenites of the first group with the low REE content. The difference between the Ta-Nb and Zr-Hf is also smaller, compared with the megacrystalline ilmenites. Phlogopites have characteristic patterns that resemble those for clinopyroxenes due to the high inclination of $(Gd/Yb)_n$. But the LREE part is flattened. This is typical of phlogopite patterns from peridotites in picrite basalts from the Vitim plateau (Ashchepkov et al., 2011).

A series of clinopyroxenes from garnet pyroxenites (Fig. 13) have a very characteristic sloping REE patterns with the rounded LREE branch. The $(Gd/Yb)_n$ ratio is higher than for Cr-diopsides from Vitim plateau (Ashchepkov et al., 2011). Garnets from the pyroxenites show rounded convex REE patterns with the hump and maximum in Dy. They are characterized by deep troughs of Ba, Sr, Pb (Pb minimum is not typical for garnets), a small dip in Zr and quite high levels of U, Ta, Nb. Garnets from metasomatites show a concave HMREE part of the pattern which is common for harzburgites from Udachnaya and other pipes (Boyd et al., 1997; Ionov et al., 2011; Ashchepkov et al., 2013b).

For the clinopyroxenes from metasomatic vein Stk167 (Fig. 13) the elevated levels of LREE and flattened LMREE part are similar to the phlogopites. The HREE part of the pattern is also is concave. As with most phlogopites, it is characterized by a high concentration of Ba. The TRE spiderdiagrams for minerals from the websterites reveal minima in Ba, Sr, and Pb. But metasomatites reveal elevated incompatible element levels especially in Rb and Ba (Matusiak-Małek et al., 2010).

7. $^{40}Ar/^{39}Ar$ ages of phlogopites

Comparing with the phlogopite ages of mantle peridotites in the Daldyn field that mainly refer to Archean events, magmatic and metasomatic events in the Alakit region refer to the middle and late Proterozoic events and the Proterozoic–Phanerozoic boundary. One of the most ancient $^{40}Ar/^{39}Ar$ ages in the mantle of Alakit is given by xenocrysts from Amakinskaya pipe (1154 Ma). Ti- and alkali-rich veins with alkaline amphiboles close to richterites in the Sytykanskaya pipe give 1015 Ma (integrated 879 Ma) (Fig. 14). Several phlogopite xenocrysts from other pipes in the Alakit field are close to 600–530 Ma. The latest event at 382 Ma is close to the beginning of the late Devonian plume event. Similar ages are also noted in other isotopic systems (Snyder et al., 1977; Pearson et al., 1997; Griffin et al., 1999a,b; Smelov and Zaitsev, 2013). As a rule it is divided from the main kimberlite appearance of the kimberlite by an interval of about 25–30 Ma.

8. Discussion

8.1. Variations structure and evolution of the mantle section

Comparison of three diagrams for ABK, PK (Fig. 10A, B) and xenoliths (Fig. 11) shows that the diagram for the ABK is more complex and probably more complete than for the PK. Some additional trends for garnets are visible in the middle part of the section as well the Chr show also more complex and extending arrays. But the major difference is in the abundance of the Cpx which in the lower part corresponds mainly to the ilmenite PT conditions and associations.

Commonly the thickness of the lithosphere beneath cratons is close to 207–250 km and eclogites are mainly determined in the lower part of mantle section (Snyder et al., 1997; Kopylova and Caro, 2004; Heaman et al., 2006; Ashchepkov et al., 2011; Smit et al., 2014). The eclogites in SCLM of Sytykanskaya (Koptil et al., 1975; Lazko et al., 1982; Spetsius and Koptil, 2008) are determined near 5 GPa and near the diamond–graphite transition. The cluster from 4 to 3.5 GPa with $Fe^{\#}$ (0.09–0.12) corresponds to the metasomatites and hybrid eclogites. But the upper part of SCLM Cpx trends nearly coincides with the PT estimates for low pressure ilmenite trend which probably trace the developing protokimberlite channels and fractionation of the protokimbelite magma. There are two subtrends for the Cpx extending to the Moho and probably reflecting the large vein associations ($Fe^{\#}$ =13–15) and accompanied metasomatites in peridotites.

The diagram for the xenoliths shows steeped structure of the mantle column especially on P-$Fe^{\#}$-$f(O_2)$ diagrams where about six nearly isobaric levels are found from 3.5 GPa to the base of the SCLM. Garnets together with Opx and most of Chr and some Cpx estimates show rather low-T geothermal branch which is close the average Arkhangelsk geotherm (Afanasiev et al., 2013) determined by the method used by Mather et al. (2011) which cut the conductive geotherms and is close to 35 mW/m^2 at 6.5 GPa and is close to 600 °C near Moho. Similar geotherm is determined for 10 Opx-Gar associations. Different configuration of the PT and P-CaO, FeO, TiO_2 etc. arrays are detected for each of mineral type. Garnets show three trends P-$Fe^{\#}$: primary $Fe^{\#}$ (6–7 wt.%) and two stages of melt percolations: 8–9 wt.% and 11 wt.%. The more Fe-rich associations within the pyroxenite layer coinciding with the Ilm metasomatites and hybrid eclogites probably reflect different metasomatic event took place in Rodinia (Santosh et al., 2009) mantle and last event lived by the protokimberlites. They show several joint trends for the Ilm and Cpx in Fe - with the $Fe^{\#}$ (~0.11 and 0.13) which is increasing in the upper part to the pyroxenite layer.

Garnet diamond inclusions PT estimates and P-Fe stepped trend reflect the primary layering consisting from at list 6 intervals in the lower part of SCLM starting from 3.5 GPa. They are also visible on the P-$f(O_2)$ diagrams where there are several lines of equal pressures but different $f(O_2)$.

The diamonds inclusions of different type mark different levels within mantle column. Most peridotitic garnet diamond inclusions of sub-calsic type refer to so cold ancient garnets (Griffin et al., 2002, 2009; Taylor and Anand, 2004; Pearson and Wittig, 2014; Pearson,

Please cite this article in press as: Ashchepkov, I.V., et al., The Sytykanskaya kimberlite pipe: Evidence from deep-seated xenoliths and xenocrysts for the evolution of the mantle beneath Alakit, Yakutia, Russia, Geoscience Frontiers (2014), http://dx.doi.org/10.1016/j.gsf.2014.08.005

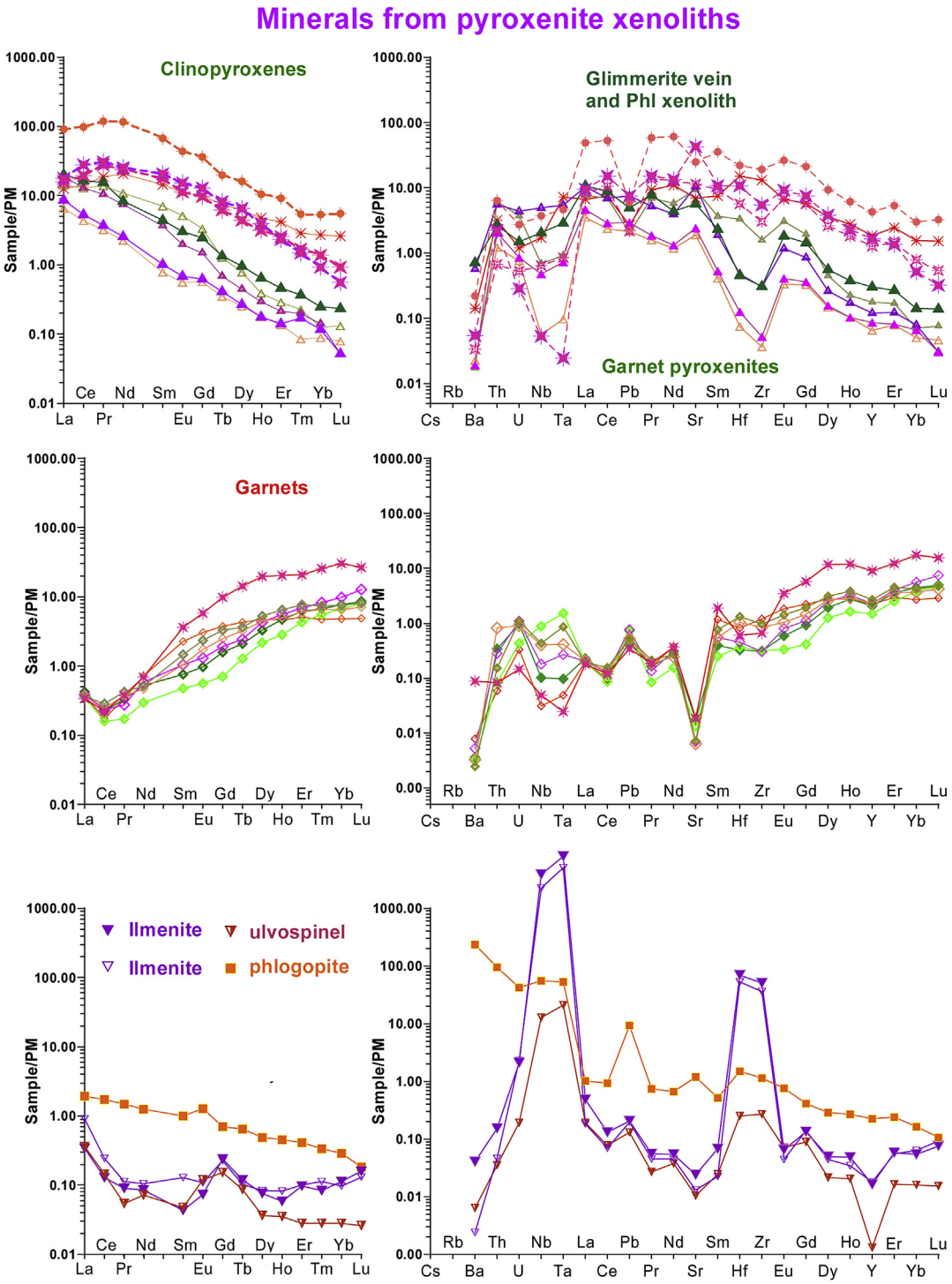

Figure 13. REE patterns and TRE spider diagrams for the minerals from pyroxenite xenoliths and alkali amphibol-bearing glimmerites from Sytykanskaya pipe (marked by asterisks).

1999) and mark 5 levels from the lithosphere base to pyroxenite layer. A few garnet diamonds inclusion are more Fe rich and coincide with the conditions determined for chromites which in pressure are closer to the chromite diamond inclusions and hot branch produced ilmenites possibly related to protokimbelite. They reveal pyroxenitic conditions enrichment in CaO showing higher $Fe^{\#}Ol$ 0.07–0.09 and may be coeval with the chromite diamond inclusions.

Pyroxene diamond inclusions and diamond eclogites which were found within 3.5–4 GPa reveal pyroxenitic affinity due to high CaO in garnets and are rather Fe rich ($Fe^{\#} = 0.25$). They are similar to kyanite CaO rich eclogites (Heaman et al., 2006). The high MgO referring to the lithosphere base like those found beneath Canada Jericho (Smart et al., 2009) at 5–5.5 GPa probably also reflect the primary mantle stratification. Later interaction with the different magma produced different types of pyroxenites (Gonzaga et al.,

Please cite this article in press as: Ashchepkov, I.V., et al., The Sytykanskaya kimberlite pipe: Evidence from deep-seated xenoliths and xenocrysts for the evolution of the mantle beneath Alakit, Yakutia, Russia, Geoscience Frontiers (2014), http://dx.doi.org/10.1016/j.gsf.2014.08.005

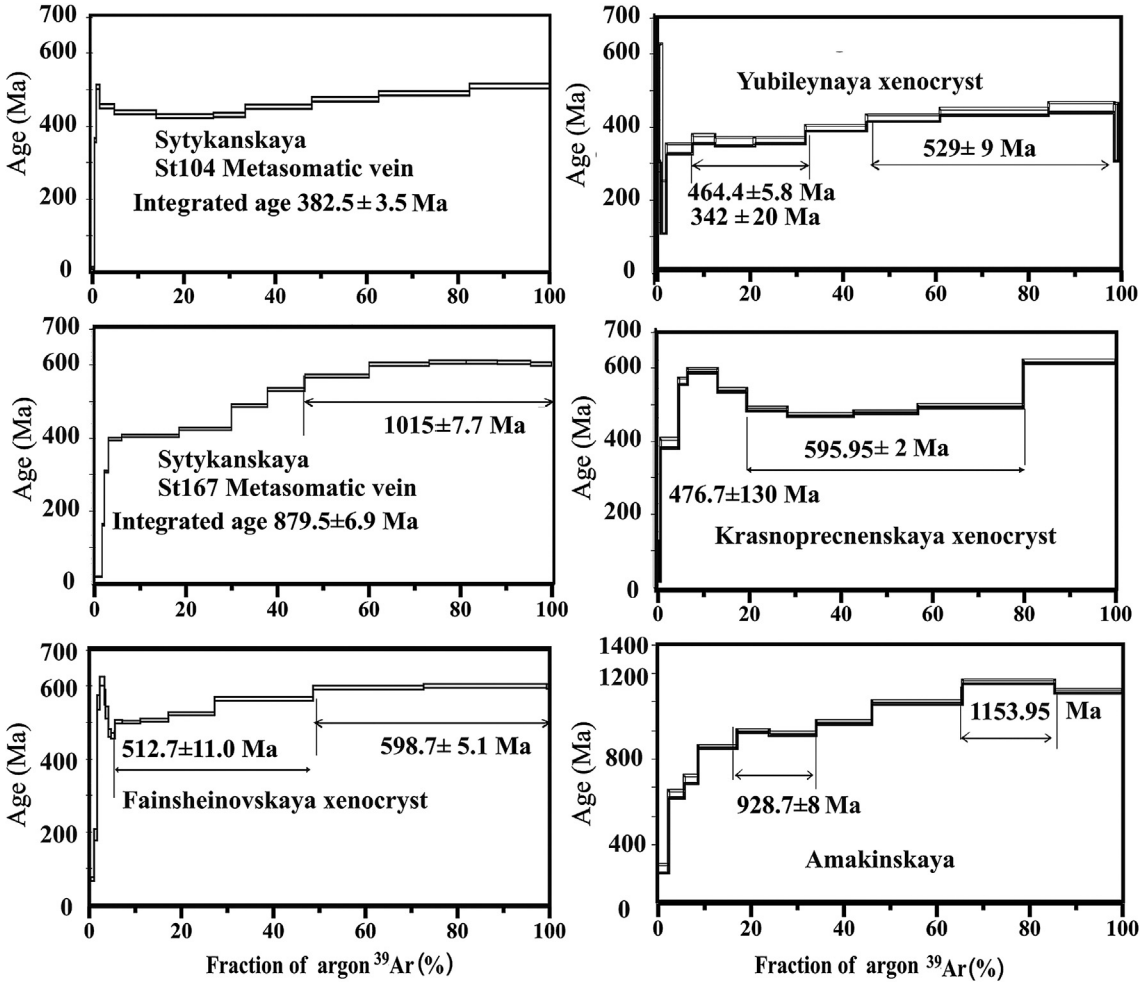

Figure 14. Ages of the phlogopites received by ^{40}Ar-^{39}Ar method for the xenoliths of Sytykanskaya pipe in comparison with the ages for the xenocrysts from Alakite kimberlite pipes.

2010) including hybrid Cr-bearing eclogites located mainly at the same levels (Spetsius and Koptil, 2008).

Cr-bearing garnet with graphite websterites are located in different levels within 40–50 GPa and some of them near Moho. A few pyroxenites are found within 6–6.5 GPa. Their position and geothermal conditions are close to those found beneath Mir (Roden et al., 2006) and Udachnaya pipe (Sobolev, 1977; Snyder et al., 1997; Pokhilenko et al., 1999).

The metasomatic horizon with the alkaline amphiboles is locating judging from the thermobarometry within the lower part of the pyroxenite layer (4–4.5 Gpa) and judging by the high alkalinity and TiO_2 content should be related to the plume event which took place at the early stage of Rodinia (Condie, 2004; Santosh et al., 2009).

The ilmenite trend for the ABK stage is more extending than for PK stage and probably reflects the transferring of the protokimberlites to the upper part of mantle section. The abrupt linear increase in this component from 2 to 3 wt.% Cr_2O_3 probably relates to the stage of the formation of the melt channels in the mantle column which was accompanied by the dissolution of the minerals from country rocks, mainly chromite and Cr-diopsides. Comparing with the PK the ilmenites from the upper part of SCLM are more Cr-rich. In the upper part the oxidation state of the ilmenites and accompanied metasomatites are rising which probably corresponds to an increase of differentiation of protokimbelrlites and metasomatism under the influence melt systems.

The complex configuration of the ilmenite trends for both stages reflects the complex structure of the feeder system for the protokimberlites which in general is divided into two levels. This TiO_2-Cr_2O_3 configuration is quite different compared with the situation of the South Africa where Cr-enrichment is common for the low- and high-Mg ilmenite varieties which was determined as Haggerty's parabola (Haggerty, 1975) explained as a structural phenomenon (which is a mistake). But in reality it is related to the metasomatites located in the upper and lower parts of the protokimberlite system. And the high enrichment in the middle part close to the pyroxenite layer is referring to the glimmerite veins.

The ilmenites from xenoliths also are marking sheared peridotites which mostly belong to the lower part of the mantle section but several PT estimates like in SCLM beneath Dalnyaya pipe (Rodionov et al., 1991) also mark intermediate levels between 65 and 35 GPa similar to the mantle section beneath Kimberly pipe (Katayama et al., 2009). This corresponds probably to the interaction with the highly enriched in volatiles melts which decrease the mechanic (Karato, 2010). Location of the clusters of Ilm-bearing metasomatites in different levels probably corresponds to the primary layering. Are they determined by the conditions of the protokimberlite rise with the periodic boiling or are they corresponding to the primary layering? Probably these are combined phenomena and dynamic of the melts upwelling is determined by the primary mantle bending. It is necessary to say that some Ilm-bearing peridotites show rather

Please cite this article in press as: Ashchepkov, I.V., et al., The Sytykanskaya kimberlite pipe: Evidence from deep-seated xenoliths and xenocrysts for the evolution of the mantle beneath Alakit, Yakutia, Russia, Geoscience Frontiers (2014), http://dx.doi.org/10.1016/j.gsf.2014.08.005

wide compositional range of ilmenites what is also common for the polymict breccias (Giuliani et al., 2013).

The Ilm-Gar wehrlites in the lithosphere base are similar to Dalnyaya to those found in the beginning of fractionation trend for protokimberlites beneath Dalnyaya pipe (Rodionov et al., 1988). The accompanied metasomatites could be diamond bearing like those found beneath Udachnaya (Pokhilenko et al., 1976) because some ilmenites were determined as inclusions in diamonds (Reimers, 1994).

The difference of the P-T-X-$f(O_2)$ configurations produced by the xenocrysts from PK and ABK concentrates and layering reconstructed by xenoliths is explanation by the fact that xenocrysts in kimberlites are mainly from the wall rocks and contact zones of the feeding channels which are influenced by the protokimberlites forming the channels of the melt path. Rather smooth trends with the several reflect the evolution of the portokimbelrlites. And this also explains the variations of xenocrysts from the PK and ABK. They reflect mainly the evolution of the contact association of protokimberlites in two stages.

The rather long Ilm-Cpx and Gar P-Fe$^{\#}$ trends may mark not only the contact associations but also the direct melt percolation through the mantle columns (Foley, 1992). But carbonate like and relatively oxidized melts s should crystallize near the graphite – diamond transitions (Tappe et al., 2006).

8.2. Trace element evidences for the magmatic and metasomatic events in mantle column beneath Sytykanskaya pipe

Geochemical features of the xenocrysts from the PK and ABK also reflect the features of the melts which reacted with the peridotite wall rocks. To see the primary features we reconstructed with KD for Cpx (Hart and Dunn, 1993; Bedard, 2006), Gar (Hauri et al., 1994; Green et al., 2000) and for ilmenites (Zack and Brumm, 1998) (Fig. 15).

Two types of the highly inclined Cpx patterns probably are produced under influence of the protokimberlites which show reduced left part of the TRE patterns similar to the megacryst from the Sloan pipe (Ashchepkov et al., 2013b). They reveal the lowering of the HFSE comparing to the REE. The Ta-Nb are essentially lower which corresponds to co-precipitation of ilmenite and possibly rutile are less evident in the reconstructed parental melt patterns. Two types of REE and TRE patterns with the different inclination $(La/Yb)_n$ are produced by the melts which precipitated (were in equilibrium) different amount of garnets and probably are derived from protokimberlites in different depth. The dips in Pb show that these melts precipitated sulfides, the only one sample has Pb, U peaks and lower REE probably have the admixture of the partial melts. The one sample components, probably was derived from the most fractionated fluid-saturated enriched melt close which did not precipitated Ilm.

The garnets from the concentrates revealed hybrid features which may be detected by the inflected patterns with the minima in HMREE part and elevated LREE part. The HFSE enriched which is common for fertilization by the carbonatite melts (Griffin et al., 1999b; Burgess and Harte, 2004; Ashchepkov et al., 2013a,b,c; Marchesi et al., 2013). We did not study the zonation with the TRE because there is possible explanation (Howarth et al., 2014) of the systematic difference TRE geochemistry between the ABK xenocrysts and minerals from xenoliths.

Many veined peridotites xenoliths from Sytykan pipe reveal the inflected pattern as with the minima in HREE and inflected patters. The contamination in wall rocks and dissolution of some minerals in the metasomatic veins created may be the reason of the inflected REE patterns.

Modeling of the melting and fractionation (Fig. 17A) shows that most of pyroxenes were produced by not a partial melts which often show low $(La/Sm)_n$ ratios when the Gar/Cpx ratio in rock is rather high. The lineal inclined patterns could be result of the melting of already enriched peridotites with very low degree ~0.01% (Fig. 17B). So most of Cpx parental melts result from the high degree of the protokimberlite differentiation.

The garnet parental melts show sometimes essential U maxima but Th and Ba enrichment which are a relic subduction sign visible in some Udachnaya peridotites (Doucet et al., 2012) but some elevated LILE components and Th are a result of the metasomatism produced by the carbonatite type melts. The Zr minima is more typical for H_2O than for carbonatite type of metasomatism, that are probably evidence for the primary harzburgitic nature or back arc - dunite associations (Fig. 15A, B).

The spectra of the melts parental for phlogopites showing the cut hump in the left part are results of crystallization from melts which had already crystallized clinopyroxenes with patterns that are humped in the LREE part.

Metasomatites and pyroxenites show similar signs of metasomatism with elevated HFSE (Fig. 16) components which commonly mark the carbonatite-related metasomatism. The glimmerites with richterites reflect the fluid-rich conditions with the essential LILE enrichments. But the lack of Sr, Pb, U anomalies probably shows that peridotite did not undergo fluid flux from a subducted slab subjected to the typical oceanic metasomatism.

Pyroxene with rounded REE spectrum “humped” in the left part belong to the common peridotites (Boyd et al., 1997; Ionov et al., 2011; Ashchepkov et al., 2013b) from the melts formed at ~0.75–1% melting degree which have not undergone interactions with metasomatic agents. The melts with the inclined REE patterns and ~100 C1 commonly were created from 1% melts of primitive mantle (McDonough and Sun, 1995; Ashchepkov et al., 2011) (Fig. 17B). So the pyroxenes from Sytykanskaya pipe correspond to a lower melting degree taking place in volatile-saturated systems. The left part reveals some variation which is likely caused by LREE fractional crystallization of clinopyroxene or AFC process. The inflection of the patterns in Gd likely reflects the process of mixing with the melt having a pattern with the opposite REE inclination which may be garnet.

The melts parental for the ilmenites are quite different in TRE (Fig. 15A, B). The low concentrations are typical for the dunite veins in the SCLM base and possibly accompanied metasomatites. The inclined patterns with the lineal REE are typical for the protokimberlites which created in the lower and middle part of mantle column. The highly enriched in TRE patterns are typical for the metasomatic Gar-bearing associations enriched in HFSE in different degrees. They also show the inflections that can possibly be explained by the dissolution of separate minerals by the highly differentiated volatile enriched melts (Fig. 16).

The dips in Ta-Nb for the melts parental for ilmenites (Fig. 15) are characteristic of the ilmenites derived from the protokimberlite melts crystallized essential amount ilmenites and garnets.

The convex REE tendencies are characteristic for the final crystallization of melts that precipitated phases with convex REE distributions. Such patterns are common for the phlogopites. Phlogopite in this same vein shows a more pronounced tilt in HREE and the LMREE.

8.3. Stages of the metasomatism

8.3.1. Ancient metasomatism

$^{40}Ar/^{39}Ar$ age suggests that there were ancient metasomatites like in mantle columns beneath Udachnaya pipe (Pokhilenko et al., 2012) which appears to be associated mainly with water-bearing

Please cite this article in press as: Ashchepkov, I.V., et al., The Sytykanskaya kimberlite pipe: Evidence from deep-seated xenoliths and xenocrysts for the evolution of the mantle beneath Alakit, Yakutia, Russia, Geoscience Frontiers (2014), http://dx.doi.org/10.1016/j.gsf.2014.08.005

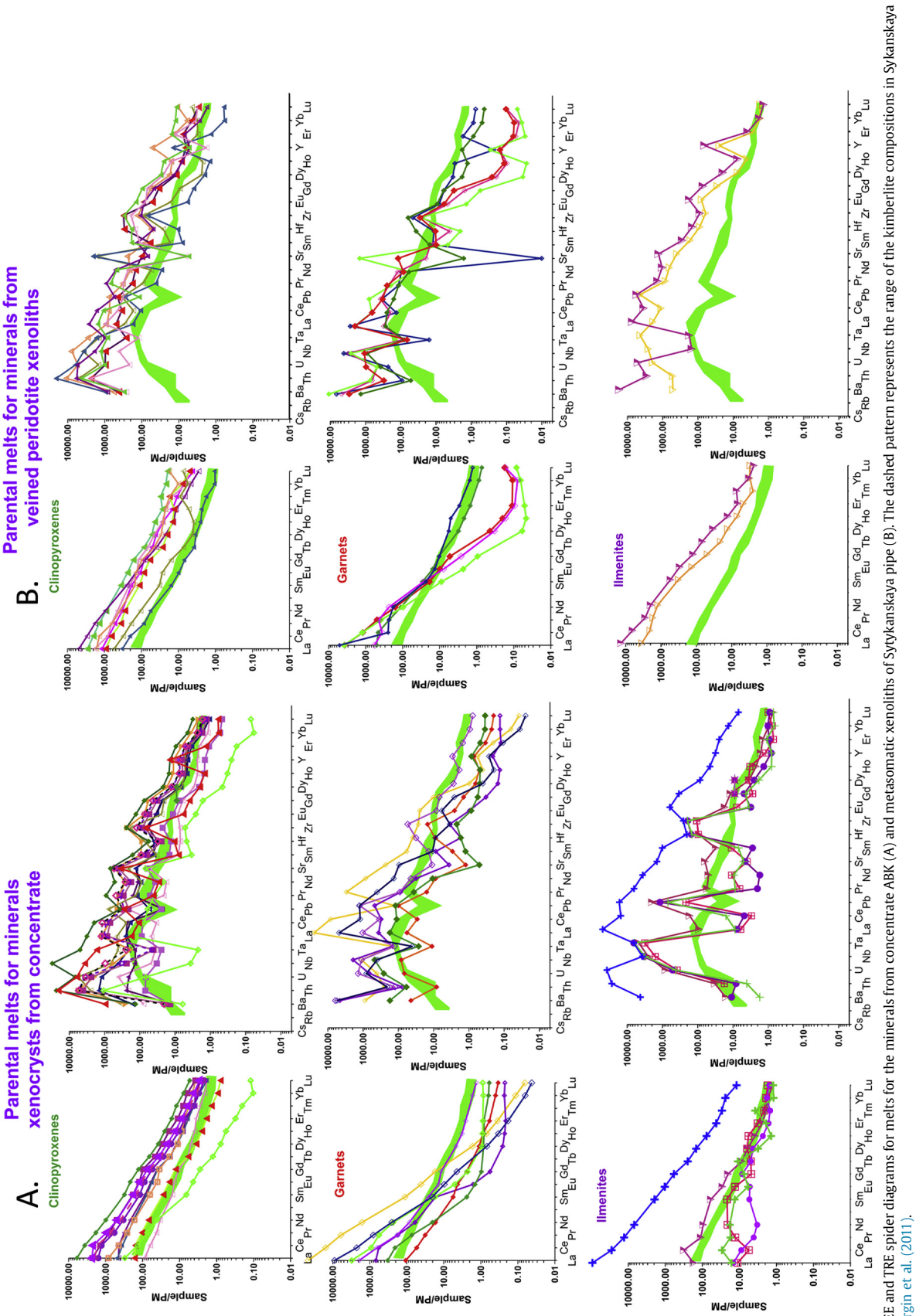

Figure 15. REE and TRE spider diagrams for melts for the minerals from concentrate ABK (A) and metasomatic xenoliths of Sytykanskaya pipe (B). The dashed pattern represents the range of the kimberlite compositions in Sykanskaya pipe after Kargin et al. (2011).

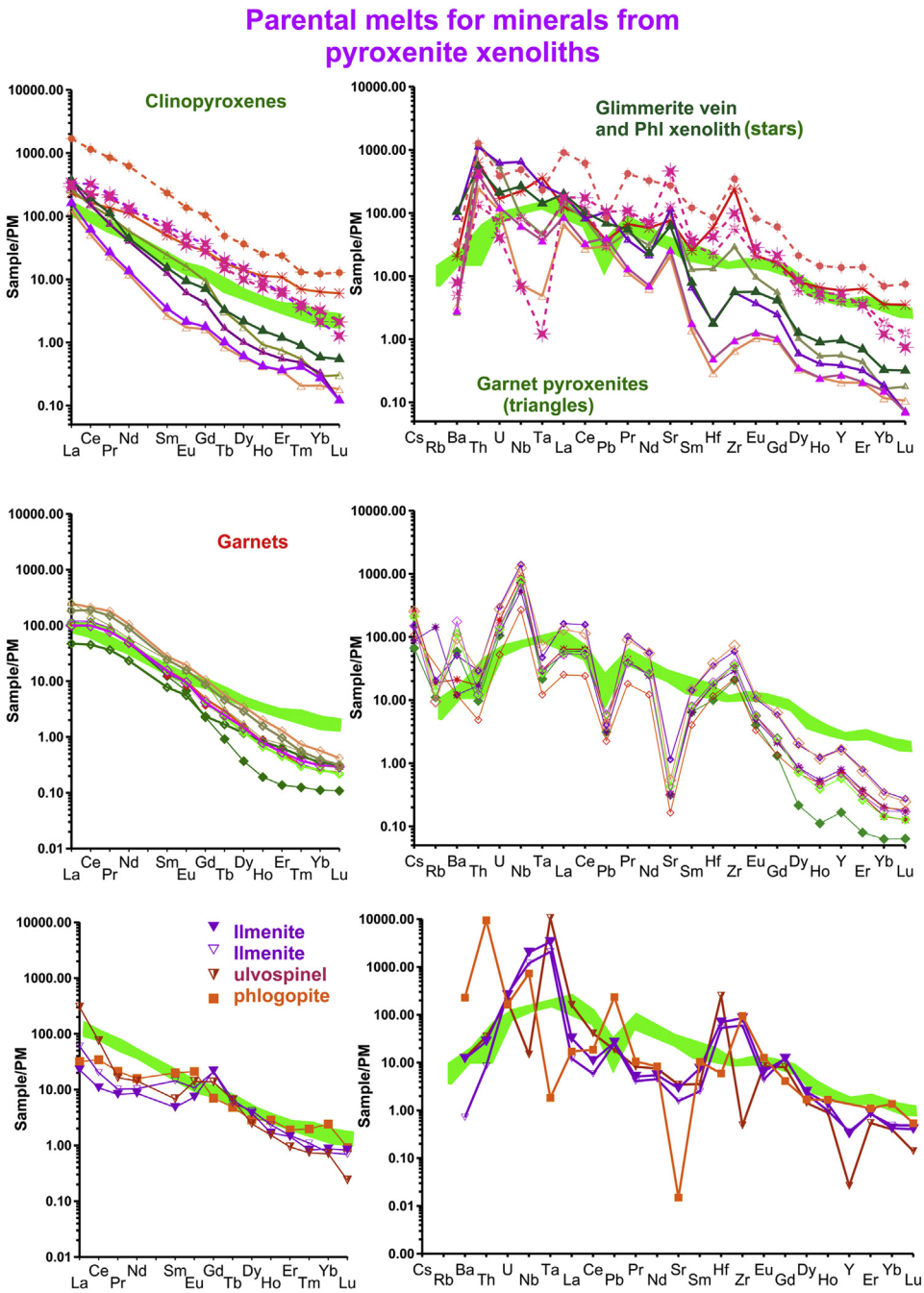

Figure 16. REE and TRE spider diagrams for melts parental for the minerals from pyroxenite xenoliths and amphibole bearing glimmerites from Sytykanskaya pipe (marked by asterisks).

highly alkaline melts and relatively young metasomatites which were produced by differentiated carbonatite-type melts. The first is probably characterized by back-arc melts (Pearson et al., 1997) with relatively high Ba, Sr, Pb, Sr, K and Na. In our case the scattered phlogopites suggest the influence of K-rich fluids which may have taken place in the marginal continental environment which should be accompanied the lamproite magmatism. But absence of HFSE anomalies means relatively reduced conditions. Formation of websterites with phlogopite and graphite which are complimentary to the ancient metasomatites with the elevated U, Ta, Nb and LILE elements should refer to this time. Presence of such pyroxenites in different levels suggests essential pervasive melt percolation (Griffin and O'Reilly, 2007) but there is no such depletion though the sinusoidal garnet REE patterns are quite common. Relatively low alkalinity and $Fe^{\#}$ is characteristic for the pyroxenes from this stage. The abundance of carbon may be sign of typical subduction processes but graphite oxygen isotope values close to average mantle values.

This type of metasomatites is in the low-Fe part of the variation diagram. Judging by the abundance of S-type garnets, almost the entire lithospheric mantle column under the Sytykanskaya pipe was subjected to large-scale phlogopite metasomatism which probably corresponds to earliest age about 1153 Ma (Fig. 14).

Please cite this article in press as: Ashchepkov, I.V., et al., The Sytykanskaya kimberlite pipe: Evidence from deep-seated xenoliths and xenocrysts for the evolution of the mantle beneath Alakit, Yakutia, Russia, Geoscience Frontiers (2014), http://dx.doi.org/10.1016/j.gsf.2014.08.005

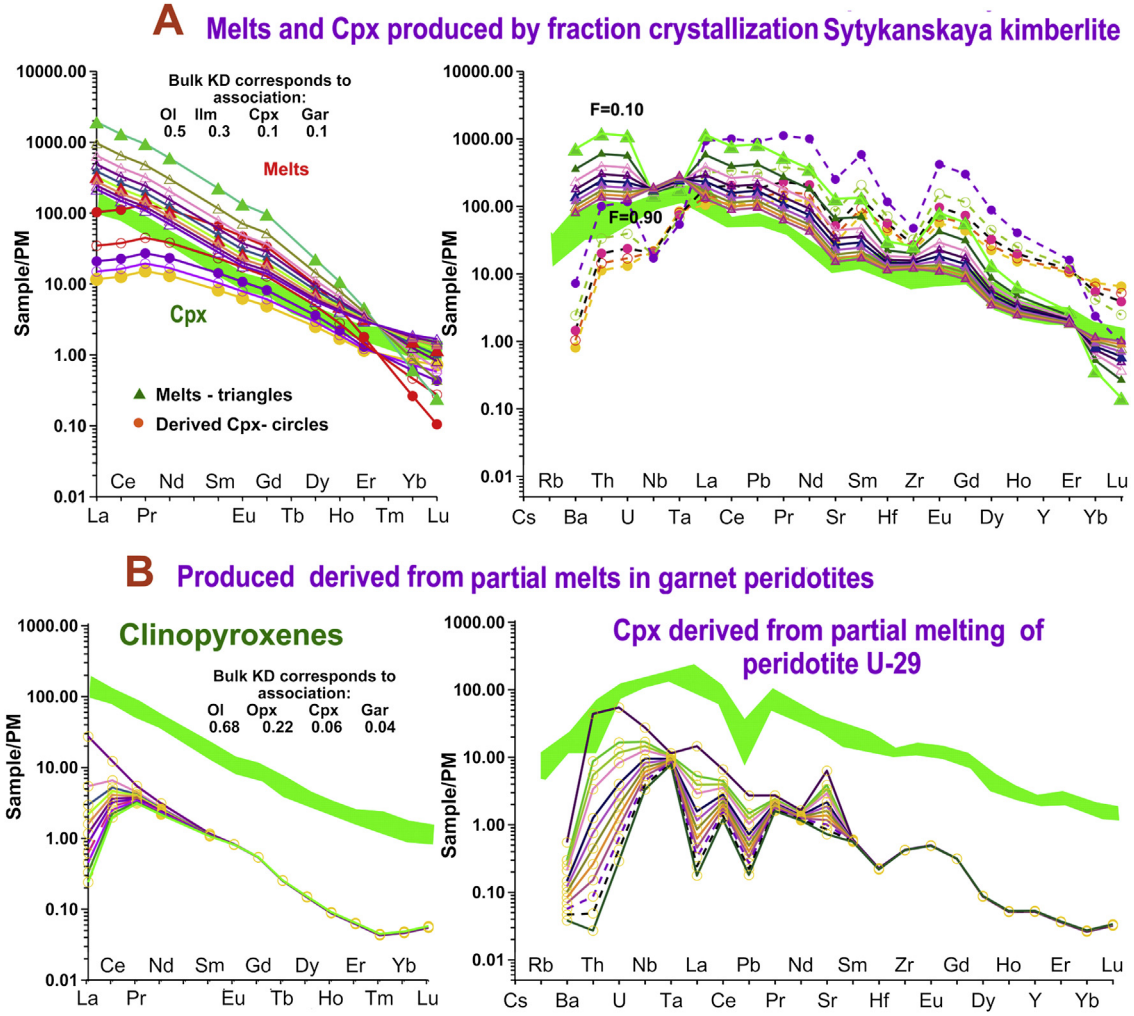

Figure 17. (A) Modeling of the partial melting of Udachnaya pipe peridotites with the bulk KD corresponding to the modal abundances (Doucet et al., 2012). (B) Fractionation of the protokimberlite melts with the bulk KD corresponding to association Ol-0.5, Ilm-0.15, Cpx-0.25, Gar-0.1. The Partition coefficients are taken from Hart and Dunn (1993), Hauri et al. (1994), Harte and Kirkley (1997), Zack and Brumm (1998), Green et al. (2000) and Bedard (2006).

The formation of highly alkaline and Ti metasomatic veins with richterite ~1015 Ma ago refers to large-scaleplume-related melt percolation in the lithospheric mantle of Rodinia (Santosh et al., 2009). Similarly in South Africa phlogopite metasomatism in mantle corresponding to 1100 Ma is associated with the plume-generated Bushveld intrusion (Hopp et al., 2008). The superplume events commonly show the correlations of the all ages for the Phl in mantle and low crust (Eccles et al., 2010).

Most of the pyroxenes from the concentrates reveal the protokimberlite features and fractionation patterns which have HFSE and Pb dips (Fig. 15A). Typical partial melts from peridotites commonly show lower inclination of REE pattern and more smoothed TRE spider diagrams (Fig. 15B). Most of metasomatic associations reveal transitional features between these two end members.

8.3.2. Plume event referring to the Rodinia supercontinent breakdown

The largest event shown in the lithosphere under many Alakit pipes took place ~600–550 Ma ago, close to the Proterozoic–Phanerozoic boundary. Such an event is close to the time of mellilite carbonatite magmatism in the Sayan Foothills and the Baikal area (Travin et al., 2002). This should correspond to the Ti-rich carbonatite-type metasomatism.

8.3.3. Protokimberlite stage

High-Fe and Ti metasomatic ilmenite veins are related to the protokimberlite melts. The amount ilmenites in the pipe are rather high. It seems that protokimberlite melts could dissolve early metasomatites in the base of mantle column. According to some works an essentially oxide liquid could form a separate phase due to immiscibility with the silicate melt (Clarke and Mackay, 1990) and, apparently, form an intrusive phase. Almost monomineral ilmenite veinlets in peridotites cut the large porphyroclusts of garnets in some xenoliths.

Furthermore, metasomatites related to the ilmenites are much more ferrous than usual peridotites. The influence of ilmenite metasomatism appears in the xenoliths sufficiently widely, although scattered Phl metasomatism dominates. It is not clear to what extent the protokimberlite melts influenced the lithospheric mantle. Did they cause changes only near the conducting channels or was it more widespread? An answer could be given by the study of xenoliths of other small pipes of this field.

Please cite this article in press as: Ashchepkov, I.V., et al., The Sytykanskaya kimberlite pipe: Evidence from deep-seated xenoliths and xenocrysts for the evolution of the mantle beneath Alakit, Yakutia, Russia, Geoscience Frontiers (2014), http://dx.doi.org/10.1016/j.gsf.2014.08.005

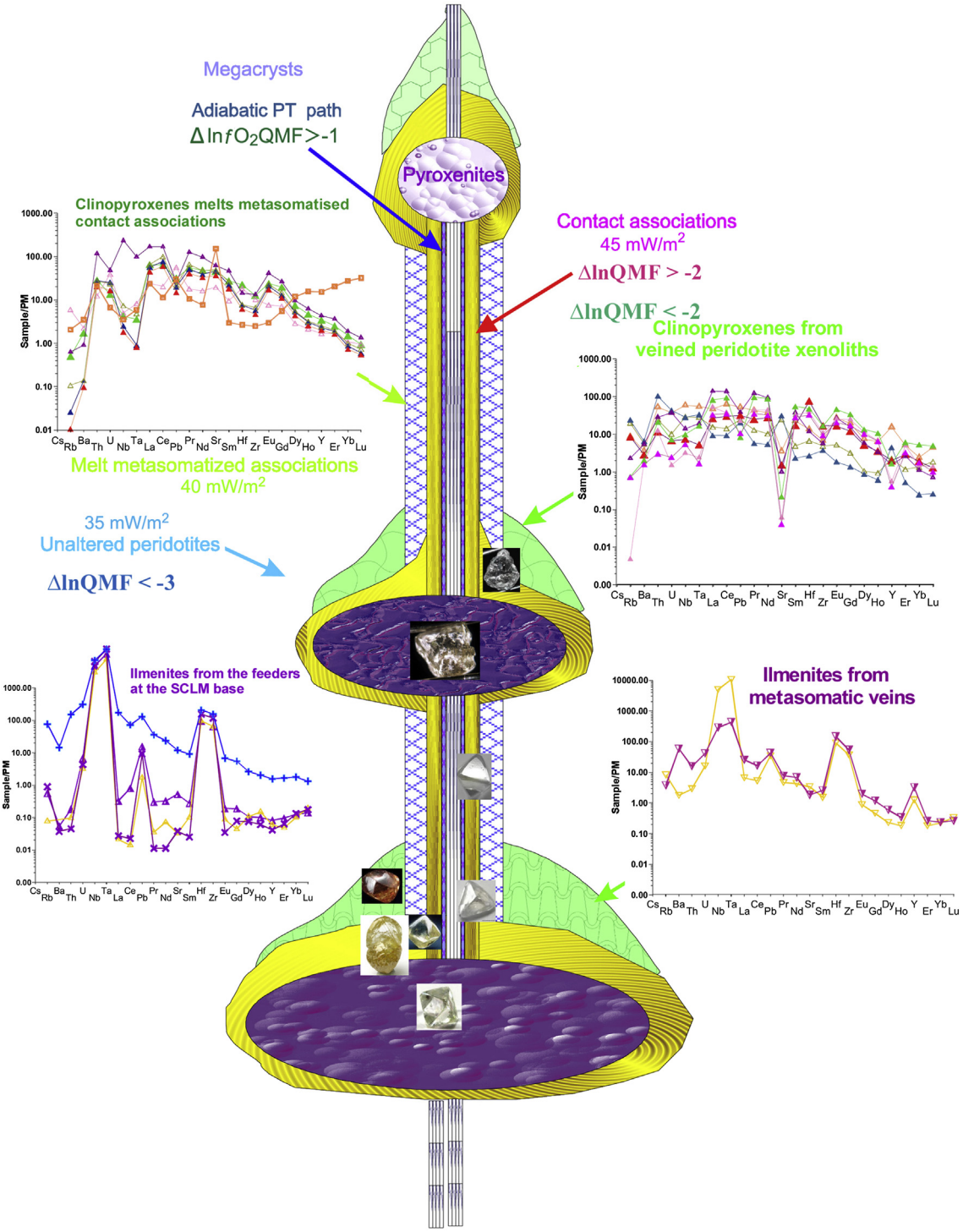

Figure 18. The scheme demonstrating the difference in the conditions of the internal zones of magma chambers and feeder systems. The inner contact should represent by essentially Cpx aggregates with the relics of garnets. The outer contacts should be represented by the veined peridotites.

The time gap of 25–30 Ma between the beginning of plume activity and mantle metasomatism and appearance of major kimberlitic explosions is documented also by other isotopic systems (Smelov and Zaitsev, 2013). However, it is not possible to discount the presence of excess argon, which can produce a more ancient age, measured only by the $^{40}Ar/^{39}Ar$ method. However, the dating of kimberlite by this method gives acceptable results (Agashev et al., 2004).

8.4. Structure of the feeder systems and the explanations

It is necessary to emphasis that many of the associations of mantle xenoliths from Sytykanskaya pipe show the signs of the disequilibriums (Reimers, 1994; Reimers et al., 1998) like those detecting in xenocryst and intergrowth from Zagadochnaya pipe (Nimis et al., 2009; Ziberna et al., 2013). They are visible not only in the veins and veinlets and rim on garnets and other reaction

Please cite this article in press as: Ashchepkov, I.V., et al., The Sytykanskaya kimberlite pipe: Evidence from deep-seated xenoliths and xenocrysts for the evolution of the mantle beneath Alakit, Yakutia, Russia, Geoscience Frontiers (2014), http://dx.doi.org/10.1016/j.gsf.2014.08.005

products which could be explained by the multistage metasomatism. There also coronas on garnets (Fig. 2, Supplementary File 1) sometimes monomineral consisting from phlogopites or ilmenites, sometimes polymineral together with the pyroxenes and chromites or ulvospinels. Some aggregates after the garnets consist from the symplectites of Phl together with Cpx, Ilm or Chr. Many garnets show reaction alteration or complete substitution which may be not only the result of reactions and dissolution but also sign of mantle diapirism which is proved by thermobarometry.

There are several possibilities to explain the wide variation of the $f(O_2)$ conditions and geochemistry of mantle xenocrysts. The internal zones for the feeders and magmatic chambers should represent the geochemistry of pure protokimberlites highly enriched in fluids (Moore and Lock, 2001; Kopylova et al., 2009) for the Cr-low or -less associations (Ol, Cpx, Ilm, Gar) showing the signs of fractionation. The outer rims should consist from the zones of the Cr-bearing associations of relatively coarse Ti enriched Cpx, with the elevate Cr content. The geochemistry of the grains should be close to the protokimberlites. Such pyroxenes are found not only in Sytykan but also are typical for the Sloan. In the outer contacts the influences of the direct intrusions should be less. But the small veinlets produced by fluid enriched melts which could be of quite variable compositions and produce dispersed intergranular Phl or ilmenites or veins of monomineral or mostly polymineral associations.

8.5. Influence of mantle metasomatism on diamond grade

Among the diamond inclusions of Sytykanskaya pipe, chromites dominate (Manakov, 2001) as in many other pipes from the Alakit field (Sobolev et al., 2003). Another widely distributed group is sub-Ca pyropes. In a subordinate quantity the high-temperature Cr-pyroxene, apparently related to the proto-kimberlite, and usual Fe-enriched Cr-diopsides (Sobolev et al., 2009) from metasomatites are found. Sub-calcic pyropes (Sobolev et al., 1973; Sobolev, 1977; Pokhilenko and Sobolev, 1995) undoubtedly came from the ancient giant-grained dunites (Pokhilenko et al., 1991), which form veins and lenses in the lithospheric mantle. The age of such garnets by analogy with others may be 3.5–2.7 billion years. But majority of grants show slightly less ancient and thus peridotites were undergone to the ancient metasomatism (Malkovets et al., 2012). The chromite diamond inclusions form an individual group. They are not frequently associated together with the pyropes and differ in PT conditions. It seems that they are closer in conditions to the ilmenites and some high-temperature and relatively ferrous pyropes. The giant-grained dunite veins with pyropes (Pokhilenko and Sobolev, 1995) and chromites have a different genesis; however, they both served as conductors of melts. Chromite dunites could be formed with the participation of the high-temperature fluid-rich melts, which, as a rule, relate to a separate stage of the protokimberlitic process. Thus, if this is correct, then a particularly large part of the diamonds of the Sytykanskaya pipe and Alakit field as a whole is connected with the protokimberlite stage. From other side the presence of the highly depleted substratum in the lower part of the lithospheric mantle is also a contributory factor for an increased diamond grade.

However, judging by the oxidation states for the ilmenites, proto-kimberlitic melts beneath the Sytykanskaya pipes were strongly oxidized, by 1 log unit higher than the diamond stability line (McCommon et al., 2001). This possibility served as the reason for the dissolution of many diamonds (Fedortchouk et al., 2005). The variations of the oxygen fugacity even in one xenoliths may be very high (Solov'eva et al., 2012) and metasomatism may be reason of the diamond growth due to the reduction of the carbonatite melts on peridotites and an opposite to the dissolution (Fig. 18).

Acknowledgments

The work is supported by RBRF grants 05-05-64718, 03-05-64146, 08-05-00524, 11-05-00060, 11-05-91060-PICS and joint research projects of IGM SB RAS and ALROSA Stock Company 77-2, 65-03, 02-05, grant of the President of Russia MK-3240.2014.5.

Appendix A. Supplementary data

Supplementary data related to this chapter can be found at http://dx.doi.org/10.1016/j.gsf.2014.08.005.

References

Afanasiev, V.P., Ashchepkov, I.V., Verzhak, V.V., O' Brien, H., Palessky, S.V., 2013. PT conditions and trace element variations of picroilmenites and pyropes from the Arkhangelsk region. Journal of Asian Earth Sciences 70–71, 45–63.

Agashev, A.M., Pokhilenko, N.P., Tolstov, A.V., Polyanichko, N.P., Mal'kovets, V.G., Sobolev, N.V., 2004. New data on age of kimberlites from Yakutian kimberlite province. Doklady Earth sciences RAN 399, 95–99.

Agashev, A.M., Ionov, D.A., Pokhilenko, N.P., Golovin, A.V., Cherepanova, Yu, Sharygin, I.S., 2013. Metasomatism in lithospheric mantle roots: constraints from whole-rock and mineral chemical composition of deformed peridotite xenoliths from kimberlite pipe Udachnaya. Lithos 160–161, 201–215.

Amshinsky, A.N., Pokhilenko, N.P., 1983. Peculiarities of the pycroilmenite compositions from Zarnitsa kimberlite pipe (Yakutia). Russian Geology and Geophysics 24 (11), 116–119.

Arai, S., 1984. Pressure-temperature dependent compositional variation of phlogopitic micas in upper mantle peridotites. Contributions to Mineralogy and Petrology 87, 260–264.

Ashchepkov, I.V., 1980. Picroilmenites from Zarnitsa Kimberlite Pipe (Diploma thesis. Novosibirsk State University). Pokhilenko N.P. Supervisor. Novosibirsk State University, p. 65.

Ashchepkov, I.V., Vladykin, N.V., Nikolaeva, I.V., Palessky, S.V., Logvinova, A.M., Saprykin, A.I., Khmel'nikova, O.S., Anoshin, G.N., 2004. Mineralogy and geochemistry of mantle inclusions and mantle column structure of the Yubileinaya kimberlite pipe, Alakit field, Yakutia. Doklady Earth Sciences RAN 395 (4), 517–523.

Ashchepkov, I.V., Pokhilenko, N.P., Vladykin, N.V., Logvinova, A.M., Kostrovitsky, S.I., Afanasiev, V.P., Pokhilenko, L.N., Kuligin, S.S., Malygina, L.V., Alymova, N.V., Khmelnikova, O.S., Palessky, S.V., Nikolaeva, I.V., Karpenko, M.A., Stagnitsky, Y.B., 2010. Structure and evolution of the lithospheric mantle beneath Siberian craton, thermobarometric study. Tectonophysics 485, 17–41.

Ashchepkov, I.V., André, L., Downes, H., Belyatsky, B.A., 2011. Pyroxenites and megacrysts from Vitim picrite-basalts (Russia): polybaric fractionation of rising melts in the mantle? Journal of Asian Earth Sciences 42, 14–37.

Ashchepkov, I.V., Rotman, A.Y., Somov, S.V., Afanasiev, V.P., Downes, H., Logvinova, A.M., Nossyko, S., Shimupi, J., Palessky, S.V., Khmelnikova, O.S., Vladykin, N.V., 2012. Composition and thermal structure of the lithospheric mantle beneath kimberlite pipes from the Catoca cluster, Angola. Tectonophysics 530–531, 128–151.

Ashchepkov, I.V., Vladykin, N.V., Ntaflos, T., Downes, H., Mitchel, R., Smelov, A.P., Rotman, A.Ya., Stegnitsky, Yu., Smarov, G.P., Makovchuk, I.V., Nigmatulina, E.N., Khmelnikova, O.S., 2013a. Regularities of the mantle lithosphere structure and formation beneath Siberian craton in comparison with other cratons. Gondwana Research 23, 4–24.

Ashchepkov, I.V., Ntaflos, T., Kuligin, S.S., Malygina, E.V., Agashev, A.M., Logvinova, A.M., Mityukhin, S.I., Alymova, N.V., Vladykin, N.V., Palessky, S.V., Khmelnikova, O.S., 2013b. Deep-seated xenoliths from the Brown Breccia of the Udachnaya Pipe, Siberia. In: Pearson, D.G., et al. (Eds.), Proceedings of 10th International Kimberlite Conference, V1, Special Issue of the Journal of the Geological Society of India, vol. 1, pp. 59–74.

Ashchepkov, I.V., Downes, H., Mitchell, R., Vladykin, N.V., Coopersmith, H., Palessky, S.V., 2013c. Wyoming craton mantle lithosphere: reconstructions based on xenocrysts from Sloan and Kelsey Lake Kimberlites. In: Proceedings of 10th International Kimberlite Conference, vol. 1. Springer India, New Delhi, pp. 13–27.

Batumike, J.M., Griffin, W.L., O'Reilly, S.Y., 2009. Lithospheric mantle structure and the diamond potential of kimberlites in southern D.R. Congo. Lithos 112 (S1), 166–176.

Bedard, J.H., 2006. A catalytic delamination-driven model for coupled genesis of Archaean crust and sub-continental lithospheric mantle. Geochimica et Cosmochimica Acta 70, 1188–1214.

Bobrievich, A.P., Bondarenko, M.N., Gnevushev, M.A., Krasov, A.M., Smirnov, G.I., Yurkevich, R.K., 1959. The Diamond Deposits of Yakutia. Gosgeoltekhizdat, Moscow, p. 527 (in Russian).

Boyd, F.R., 1973. A pyroxene geotherm. Geochimica et Cosmochimica Acta 37, 2533–2546.

Boyd, F.R., 1990. Mantle Metasomatism: Evidence from a MARID–Harzburgite Compound Xenolith. Carnegie Institution Washington, pp. 18–23. Yearbook, 90.
Boyd, F.R., Pokhilenko, N.P., Pearson, D.G., Mertzman, S.A., Sobolev, N.V., Finger, L.W., 1997. Composition of the Siberian cratonic mantle: evidence from Udachnaya peridotite xenoliths. Contributions to Mineralogy and Petrology 128 (2–3), 228–246.
Brey, G.P., Kohler, T., 1990. Geothermobarometry in four-phase lherzolites. II. New thermobarometers, and practical assessment of existing thermobarometers. Journal of Petrology 31, 1353–1378.
Burgess, S.R., Harte, B., 2004. Tracing lithosphere evolution through the analysis of heterogeneous G9-G10 garnets in peridotite xenoliths, II: REE chemistry. Journal of Petrology 45, 609–634.
Clarke, D.B., Mackay, R.M., 1990. An ilmenite-garnet-clinopyroxene nodule from Matsoku: evidence of oxide-rich liquid immiscibility in Kimberlites? Canadian Mineralogist 28, 229–239.
Condie, K.C., 2004. Supercontinents and superplume events: distinguishing signals in the geologic record. Physics of the Earth and Planetary Interiors 146, 319–332.
Dawson, J.B., 1980. Kimberlites and Their Xenoliths. Springer-Verlag, Berlin, p. 252.
Dawson, J.B., Smith, J.V., 1977. The MARID (mica–amphibole–rutile–ilmenite–diopside)suite of xenoliths in kimberlite. Geochimica et Cosmochimica Acta 41, 309–323.
Dawson, J.B., Smith, J.V., 1982. Mantle amphiboles - a review. Mineralogical Magazine 45, 35–46.
Day, H.W., 2012. A revised diamond-graphite transition curve. American Mineralogist 97, 52–62.
Doucet, L.S., Ionov, D.A., Golovin, A.V., Pokhilenko, N.P., 2012. Depth, degrees and tectonic settings of mantle melting during craton formation: inferences from major and trace element compositions of spinel harzburgite xenoliths from the Udachnaya kimberlite, central Siberia. Earth and Planetary Science Letters 359–360, 206–218.
Eccles, D.R., Simonetti, S.S., Cox, R., 2010. Garnet pyroxenite and granulite xenoliths from or the astern Alberta: evidence of ~1.5 Ga lower crust and mantle in western Laurentia. Precambrian Research 177, 339–354.
Efimova, E.S., Sobolev, N.V., 1977. Abundance of crystalline inclusions in Yakutian diamonds. Doklady Akademii Nauk SSSR 237, 1475–1478 (in Russian).
Fedortchouk, Y., Canil, D., Carlson, J.A., 2005. Dissolution forms inLac de Gras diamonds and their relationship to the temperature and redox state of kimberlite magma. Contributions to Mineralogy and Petrology 150, 54–69.
Foley, S.F., 1992. Vein-plus-wall-rock melting mechanism in the lithosphere and the origin of potassic alkaline magmas. Lithos 28, 435–453.
Gibson, S.A., Malarkey, J., Day, J.A., 2008. Melt depletion and enrichment beneath the western Kaapvaal Craton: evidence from Finsch peridotite xenoliths. Journal of Petrology 49, 1817–1852.
Giuliani, A., Kamenetsky, V.S., Kendrick, M.A., Phillips, D., Wyatt, B.A., Maas, R., 2013. Oxide, sulphide and carbonate minerals in a mantle polymict breccia: metasomatism by proto-kimberlite magmas, and relationship to the kimberlite megacrystic suite. Chemical Geology 353 (30), 4–18.
Goncharov, A.G., Ionov, D.A., Doucet, L.S., Pokhilenko, L.N., 2012. Thermal state, oxygen fugacity and C-O-H fluid speciation in cratonic lithospheric mantle: new data on peridotite xenoliths from the Udachnaya kimberlite, Siberia. Earth and Planetary Science Letters 357–358, 99–110.
Gonzaga, R.G., Lowry, D., Jacob, D.E., LeRoex, A., Schulze, D., Menzies, M.A., 2010. Eclogites and garnet pyroxenites: similarities and differences. Journal of Volcanology and Geothermal Research 190, 235–247.
Green, T.H., Blundy, J.D., Adam, J., Yaxley, G.M., 2000. SIMS determination of trace element partition coefficients between garnet, clinopyroxene and hydrous basaltic liquids at 2–7.5 GPa and 1080–1200 °C. Lithos 53, 165–187.
Gregoire, M., Bell, D.R., Le Roex, A.P., 2002. Trace element geochemistry of phlogopite-rich mafic mantle xenoliths: their classification and their relationship to phlogopite-bearing peridotites and kimberlites revisited. Contributions to Mineralogy and Petrology 142, 603–625.
Gregoire, M., Bell, D.R., Le Roex, A.P., 2003. Garnet lherzolites from the Kaapvaal Craton (South Africa): trace element evidence for a metasomatic history. Journal of Petrology 44, 629–657.
Griffin, W.L., O'Reilly, S.Y., 2007. Cratonic lithospheric mantle: is anything subducted? Episodes 30, 43–53.
Griffin, W.L., Ryan, C.G., Kaminsky, F.V., O'Reilly, S.Y., Natapov, L.M., Win, T.T., Kinny, P.D., Ilupin, I.P., 1999a. The Siberian lithosphere traverse: mantle terranes and the assembly of the Siberian Craton. Tectonophysics 310, 1–35.
Griffin, W.L., Shee, S.R., Ryan, C.G., Win, T.T., Wyatt, B.A., 1999b. Harzburgite to lherzolite and back again: metasomatic processes in ultramafic xenoliths from the Wesselton kimberlite, Kimberley, South Africa. Contributions to Mineralogy and Petrology 134, 232–250.
Griffin, W.L., Spetsius, Z.V., Pearson, N.J., O'Reilly, S.Y., 2002. In-situ Re-Os analysis of sulfide inclusions in kimberlite olivine: new constraints on depletion events in the Siberian lithospheric mantle. Geochemistry, Geophysics, Geosystems 3 (11), 1069. http://dx.doi.org/10.1029/2001GC000287.
Griffin, W.L., O'Reilly, S.Y., Afonso, J.C., Begg, G.C., 2009. The composition and evolution of lithospheric mantle: a reevaluation and its tectonic implications. Journal of Petrology 50, 1185–1204.
Haggerty, S.E., 1975. The chemistry and genesis of opaque minerals in kimberlite. Physics and Chemistry of the Earth. New York 9, 227–243.
Hart, S.R., Dunn, T., 1993. Experimental cpx/melt partitioning of 24 trace elements. Contributions to Mineralogy and Petrology 113, 1–8.
Harte, B., Kirkley, M.B., 1997. Partitioning of trace elements between clinopyroxene and garnet: data from mantle eclogites. Chemical Geology 136, 1–24.
Hauri, E.H., Wagner, T.P., Grove, T.L., 1994. Experimental and natural partitioning of Th, U, Pb and other trace elements between garnet, clinopyroxene and basaltic melts. Chemical Geology 117, 149–166.
Hawthorne, F.C., Oberti, R., 2007. Classification of the amphiboles. In: Rosso, J.J. (Ed.), Amphiboles: Crystal Chemistry, Occurrence, and Health Issues, Reviews in Mineralogy and Geochemistry, vol. 67. Mineralogical Society of America and The Geochemical Society, Washington, DC, pp. 55–88.
Heaman, L.M., Creaser, R.A., Cookenboo, H.O., Chacko, T., 2006. Multistage modification of the northern slave mantle lithosphere evidence from zircon- and diamond-bearing eclogite xenoliths entrained in Jericho Kimberlite, Canada. Journal of Petrology 47, 821–858.
Hopp, J., Trieloff, M., Brey, G.P., Woodland, A.B., Simon, N.S.C., Wijbrans, J.R., Siebel, W., Reitter, E., 2008. $^{40}Ar/^{39}Ar$-ages of phlogopite in mantle xenoliths from South African kimberlites: evidence for metasomatic mantle impregnation during the Kibaran orogenic cycle. Lithos 106, 351–364.
Howarth, G.H., Barry, P.H., Pernet-Fisher, J.F., Baziotis, I.P., Pokhilenko, N.P., Pokhilenko, L.N., Bodnar, R.J., Taylor, L.A., Agashev, A.M., 2014. Superplume metasomatism: evidence from Siberian mantle xenoliths. Lithos 184–187, 209–224.
Ionov, D.A., Doucet, L.S., Ashchepkov, I.V., 2010. Composition of the lithospheric mantle in the Siberian Craton: new constraints from fresh peridotites in the Udachnaya-East Kimberlite. Journal of Petrology 51, 2177–2210.
Ionov, D.A., Doucet, L.S., Carlson, R.W., Pokhilenko, N.P., Golovin, A.V., Ashchepkov, I.V., 2011. Peridotite xenolith inferences on the formation and evolution of the central Siberian cratonic mantle. In: Goldschmidt Conference Abstracts, p. 1085.
Ionov, D.A., Bénard, A., Plechov, P.Yu., Shcherbakov, V.D., 2013. Along-arc variations in lithospheric mantle compositions in Kamchatka, Russia: first trace element data on mantle xenoliths from the Klyuchevskoy Group volcanoes. Journal of Volcanology and Geothermal Research 263, 122–131.
Karato, S., 2010. Rheology of the Earth's mantle: a historical review. Gondwana Research 18, 17–45.
Kargin, A.V., Golubeva, Yu.Yu., Kononova, V.A., 2011. Kimberlites of the Daldyn-Alakit region (Yakutia): spatial distribution of the rocks with different chemical characteristics. Petrology 19 (5), 496–520.
Katayama, I., Suyama, Y., Ando, S., Komiya, T., 2009. Mineral chemistry and P–T condition of granular and sheared peridotite xenoliths from Kimberley, South Africa: origin of the textural variation in the cratonic mantle. Lithos 109, 333–340.
Kennedy, C.S., Kennedy, G.C., 1976. The equilibrium boundary between graphite and diamond. Journal of Geophysical Research 81, 2467–2470.
Konzett, J., Ulmer, P., 1999. The stability of hydrous potassic phases in Lherzolitic Mantle—an experimental study to 9·5 GPa in simplified and natural bulk compositions. Journal of Petrology 40, 629–652.
Konzett, J., Armstrong, R.A., Günther, D., 2000. Modal metasomatism in the Kaapvaal craton lithosphere: constraints on timing and genesis from U–Pb zircon dating of metasomatized peridotites and MARID-type xenoliths. Contributions to Mineralogy and Petrology 139, 704–719.
Konzett, J., Wirth, R., Hauzenberger, C., Whitehouse, M., 2013. Two episodes of fluid migration in the Kaapvaal Craton lithosphericmantle associated with Cretaceous kimberlite activity: evidence from a harzburgite containing a unique assemblage of metasomatic zirconium-phases. Lithos 182–183, 165–184.
Koptil, V.I., Las'ko, E.E., Serenko, V.P., 1975. Diamond kyanite eclogites from Sytykanskaya kimberlite pipe – first finding in USSA. Doklady Earth Sciences SSSR 225 (4), 924–927.
Kopylova, M.G., Caro, G., 2004. Mantle xenoliths from the Southeastern Slave craton: evidence for chemical zonation in a thick, cold lithosphere. Journal of Petrology 45, 1045–1067.
Kopylova, M.G., Russell, J.K., Cookenboo, H., 1999. Petrology of peridotite and pyroxenite xenoliths from the Jericho kimberlite: implications for the thermal state of the mantle beneath the Slave craton, northern Canada. Journal of Petrology 40, 79–104.
Kopylova, M.G., Nowell, G.M., Pearson, D.G., Markovic, G., 2009. Crystallization of megacrysts from protokimberlitic fluids: geochemical evidence from high-Cr megacrysts in the Jericho kimberlite. Lithos 112S, 284–295.
Kostrovitsky, S.I., Alymova, N.V., Yakovlev, D.A., Serov, I.V., Ivanov, A.S., Serov, V.P., 2006. Specific features of picroilmenite composition in various diamondiferous fields of the Yakutian province. Doklady Earth Sciences 406, 19–23.
Kostrovitsky, S.I., Morikiyo, T., Serov, I.V., Yakovlev, D.A., Amirzhanov, A.A., 2007. Isotope-geochemical systematics of kimberlites and related rocks from the Siberian Platform. Russian Geology and Geophysics 48, 272–290.
Lavrent'ev, YuG., Usova, L.V., Kuznetsova, A.I., Letov, S.V., 1987. X-ray spectral quant metric microanalysis of the most important minerals of kimberlites. Russian Geology and Geophysics 48 (5), 75–81.
Lazarov, M., Brey, G.P., Stefan Weyer, S., 2012. Evolution of the South African mantle — a case study of garnet peridotites from the Finsch diamond mine (Kaapvaal craton); part 1: inter-mineral trace element and isotopic equilibrium. Lithos 154, 193–209.
Lazko, E.E., Serenko, V.P., Koptil, V.I., Rudnizkaya, E.S., Zepin, V.I., 1982. Kyanite diamondiferous eclogites from the kimberlite pipe Sytykanskaya (Yakutia). Izvestiya AN SSSR, Serlya Geologlcheskaya 7, 55–69.

Please cite this article in press as: Ashchepkov, I.V., et al., The Sytykanskaya kimberlite pipe: Evidence from deep-seated xenoliths and xenocrysts for the evolution of the mantle beneath Alakit, Yakutia, Russia, Geoscience Frontiers (2014), http://dx.doi.org/10.1016/j.gsf.2014.08.005

Logvinova, A.M., Ashchepkov, I.V., 2008. Diamond inclusions and eclogites thermobarometry, Siberia. Goldschmidt conference abstracts. Geochimica et Cosmochimica Acta. Special Supplement 72 (16S), A567.

Logvinova, A.M., Taylor, L.A., Floss, C., Sobolev, N.V., 2005. Geochemistry of multiple diamond inclusions of harzburgitic garnets as examined in situ. International Geology Review 47, 1223–1233.

Malkovets, V.G., Griffin, W.L., Pearson, N.J., Rezvukhin, D.I., O'Reilly, S.Y., Pokhilenko, N.P., Garanin, V.K., Spetsius, Z.V., Litasov, K.D., 2012. Late metasomatic addition of garnet to the SCLM: Os-isotope evidence. In: Goldschmidt conference abstracts, p. 1315.

Manakov, A.V., 2001. Material models of the upper mantle of Yakutian diamond-bearing province. Herald of the Voronezh University 11, 46–54 (in Russian).

Marchesi, C., Garrido, C.J., Bosch, D., Bodinier, J.-L., Gervilla, F., Hidas, K., 2013. Mantle refertilization by melts of crustal-derived garnet pyroxenite: evidence from the Ronda peridotite massif, southern Spain. Earth and Planetary Science Letters 362, 66–75.

Mather, K.A., Pearson, D.G., McKenzie, D., Kjarsgaard, B.A., Priestley, K., 2011. Constraints on the depth and thermal history of cratonic lithosphere from peridotite xenoliths, xenocrysts and seismology. Lithos 125, 729–742.

Matusiak-Małek, M., Puziewicz, J., Ntaflos, T., Grégoire, M., Downes, H., 2010. Metasomatic effects in the lithospheric mantle beneath the NE Bohemian Massif: a case study of Lutynia (SW Poland) peridotite xenoliths. Lithos 117, 49–60.

McCammon, C.A., Griffin, W.L., Shee, S.R., O'Neill, H.S.C., 2001. Oxidation during metasomatism in ultramafic xenoliths from the Wesselton kimberlite, South Africa: implications for the survival of diamond. Contributions to Mineralogy and Petrology 141, 287–296.

McDonough, W.F., Sun, S.-S., 1995. The composition of the Earth. Chemical Geology 120, 223–253.

McGregor, I.D., 1974. The system MgO-SiO_2-Al_2O_3: solubility of Al_2O_3 in enstatite for spinel and garnet peridotite compositions. American Mineralogist 59, 110–119.

Misra, K.C., Anand, M., Taylor, L.A., Sobolev, N.V., 2004. Multi-stage metasomatism of diamondiferous eclogite xenoliths from the Udachnaya kimberlite pipe, Yakutia, Siberia. Contributions to Mineralogy and Petrology 146, 696–714.

Mitchell, R.H., 1995. Kimberlites, Orangeites, and Related Rocks. Plenum Press, New York, pp. 1–90.

Moore, A.E., Lock, N.P., 2001. The origin of mantle-derived megacrysts and sheared peridotites-evidence from kimberlites in the northern Lesotho—Orange Free State (South Africa) and Botswana pipe clusters. South Africa Journal of Geology 104, 23–38.

Niida, K., Green, D.H., 1999. Stability and chemical composition of pargasitic amphibole in MORB pyrolite underupper mantle conditions. Contributions to Mineralogy and Petrology 135, 18–40.

Nimis, P., Taylor, W., 2000. Single clinopyroxene thermobarometry for garnet peridotites. Part I. Calibration and testing of a Cr-in-Cpx barometer and an enstatite-in-Cpx thermometer. Contributions to Mineralogy and Petrology 139, 541–554.

Nimis, P., Zanetti, A., Dencker, I., Sobolev, N.V., 2009. Major and trace element composition of chromian diopsides from the Zagadochnaya kimberlite (Yakutia, Russia): metasomatic processes, thermobarometry and diamond potential. Lithos 112, 397–412.

O'Neill, H.St.C., Wood, B.J., 1979. An experimental study of Fe-Mg-partitioning between garnet and olivine and its calibration as a geothermometer. Contributions to Mineralogy and Petrology 70, 59–70.

O'Neill, H. St. C., Wall, V.J., 1987. The olivine orthopyroxene-spinel oxygen geobarometer, the nickel precipitation curve, and the oxygen fugacity of the earth's upper mantle. Journal of Petrology 28, 1169–1191.

Pearson, D.G., 1999. The age of continental roots. Lithos 48, 171–194.

Pearson, D.G., Wittig, N., 2014. The Formation and Evolution of Cratonic Mantle Lithosphere – Evidence from Mantle Xenoliths. Treatise on Geochemistry, Second ed. Elsevier, pp. 255–292.

Pearson, D.G., Snyder, G.A., Shirey, S.B., Taylor, L.A., Carlson, R.W., Sobolev, N.V., 1995. Archaean Re-Os age for Siberian eclogites and constraints on Archaean tectonics. Nature 374, 711–713.

Pearson, D.G., Kelley, S.P., Pokhilenko, N.P., Boyd, F.R., 1997. Laser $^{40}Ar/^{39}Ar$ analyses of phlogopites from southern African and Siberian kimberlites and their xenoliths: constraints on eruption ages, melt degassing and mantle volatile composition. Russian Geology and Geophysics 38, 106–117.

Pernet-Fisher, J.F., Howarth, G.H., Liu, Y., Barry, P.H., Carmody, L., Valley, J.W., Bodnar, R.J., Spetsius, Z.V., Taylor, L.A., 2014. Komsomolskaya diamondiferous eclogites: evidence for oceanic crustal protoliths. Contributions to Mineralogy and Petrology 167, 981. http://dx.doi.org/10.1007/s00410-014-0981-y.

Pokhilenko, N.P., Sobolev, N.V., 1995. Mineralogical criteria for kimberlite diamond grade. In: Kimberlites of Yakutia: Field Guide Book: Sixth International Kimberlite Conference. Novosibirsk, pp. 79–81.

Pokhilenko, L.N., Alifirova, T.A., Yudin, D.S., 2012. $^{40}Ar/^{39}Ar$ dating of phlogopite of mantle xenoliths from kimberlite pipes of Yakutia: evidence for deep ancient metasomatism of the Siberian platform. In: 10th International Kimberlite Conference (Bangalore, India, 6–11 February, 2012): Long Abstracts. Bangalore, p. 57.

Pokhilenko, N.P., Sobolev, N.V., Sobolev, V.S., Lavrentiev, Y.G., 1976. Xenoliths of diamond bearing ilmenite-pyrope lherzolites from the kimberlite pipe Udachnaya (Yakutia). Doklady AN SSSR 231, 438–442.

Pokhilenko, N.P., Pearson, D.G., Boyd, F.R., Sobolev, N.V., 1991. Megacrystalline Dunites: Sources of Siberian Diamonds. Carnegie Institute Washington, pp. 11–18. Yearbook. 90.

Pokhilenko, N.P., Sobolev, N.V., Kuligin, S.S., Shimizu, N., 1999. Peculiarities of distribution of pyroxenite paragenesis garnets in Yakutian kimberlites and some aspects of the evolution of the Siberian craton lithospheric mantle. In: Proceedings of the VII International Kimberlite Conference. The P.H. Nixon Volume, pp. 690–707.

Ponomarenko, A.I., Spetsius, Z.V., 1976. Diamondiferous eclogites from the kimberlite pipe Sytykanskaya. Geology and Geophysics 6, 103–106.

Reimers, L.F., 1994. Deep Seated Mineral Associations of the Kimberlites Pipe Sytycanskaya (Materials of the Study of Mantle Rock and Crystalline Inclusions in Diamonds). Institute of Geology and Geophysics, Novosibirsk, p. 258.

Reimers, L.F., Pokhilenko, N.P., Yefimova, E.S., Sobolev, N.V., 1998. Ultramafic mantle assemblages from Sytykanskaya Kimberlite Pipe (Yakutia). In: Seventh International Kimberlite Conference, Cape Town, April 1998: Extended Abstracts, Cape Town, pp. 730–732.

Roden, M.F., Patiño-Douce, A.E., Jagoutz, E., Laz'ko, E.E., 2006. High pressure petrogenesis of Mg-rich garnet pyroxenites from Mir kimberlite, Russia. Lithos 90 (1–2), 77–91.

Rodionov, A.S., Amshinsky, Pokhilenko, N.P., 1988. Ilmenite – Pyrope wehrlite – a new type of kimberlite xenoliths paragenesis. Russian Geology and Geophysics 19 (7), 53–57.

Rodionov, A.S., Sobolev, N.V., Pokhilenko, N.P., Suddaby, P., Amshinsky, A.N., 1991. Ilmenite-bearing peridotites and megacrysts from Dalnaya kimberlite pipe, Yakutia. In: Fifth International Kimberlite Conference: Extended Abstracts, United States, pp. 339–341.

Rudnick, R.L., McDonough, W.F., O'Connell, R.J., 1998. Thermal structure, thickness and composition of continental lithosphere. Chemical Geology 145, 395–411.

Santosh, M., Maruyama, S., Yamamoto, A., 2009. The making and breaking of supercontinents: some speculations based on superplumes, super downwelling and the role of tectosphere. Gondwana Research 15, 324–341.

Smart, K.A., Heaman, M., Chacko, T., Simonetti, A., Kopylova, M., Mah, D., Daniels, D., 2009. The origin of high-MgO diamond eclogites from the Jericho Kimberlite. Canada Earth and Planetary Science Letters 284, 527–537.

Smelov, A.P., Zaitsev, A.I., 2013. The age and localization of Kimberlite magmatism in the Yakutian Kimberlite Province: constraints from isotope geochronology—an overview. In: Pearson, D.G., et al. (Eds.), Proceedings of 10th International Kimberlite Conference, Special Issue of the Journal of the Geological Society of India, vol. 1, pp. 225–234.

Smit, K.V., Stachel, T., Creaser, R.A., Ickert, R.B., DuFrane, S.A., Stern, R.A., Seller, M., 2014. Origin of eclogite and pyroxenite xenoliths from the Victor kimberlite, Canada, and implications for Superior craton formation. Geochimica et Cosmochimica Acta 125, 308–337.

Snyder, M., TaylorL, A., Crozaz, G., Halliday, A.N., Beard, B.L., Sobolev, V.N., Sobolev, N.V., 1997. The origin of Yakutian eclogite xenoliths. Journal of Petrology 38, 85–113.

Sobolev, N.V., 1977. Deep-Seated Inclusions in Kimberlites and the Problem of the Composition of the Mantle. Amer. Geophys. Union, Washington, DC, p. 279.

Sobolev, N.V., Lavrentev, Y.G., Pokhilenko, N.P., Usova, L.V., 1973. Chrome-rich garnets from the Kimberlites of Yakutia and their parageneses. Contributions to Mineralogy and Petrology 40, 39–52.

Sobolev, N.V., Pokhilenko, N.V., Efimova, E.S., 1984. Xenoliths of diamond bearing peridotites in kimberlites and problem of the diamond origin. Russian Geology and Geophysics 25 (12), 63–80.

Sobolev, N.V., Logvinova, A.M., Zedgenizov, D.A., Yefimova, E.S., Taylor, L.A., Promprated, P., Koptil, V.I., Zinchuk, N.N., 2003. Mineral inclusions in diamonds from Komsomolskaya and Krasnopresnenskaya Pipes, Yakutia: evidence for deep lithospheric Heterogeneities in Siberian Craton. In: 8th International Kimberlite Conference, Victoria, BC, Canada, June 22–27th. Extended Abstracts, 2003, FLA_0141.

Sobolev, N.V., Logvinova, A.M., Zedgenizov, D.A., Seryotkin, Y.V., Yefimova, E.S., Floss, C., Taylor, L.A., 2004. Mineral inclusions in microdiamonds and macrodiamonds from kimberlites of Yakutia: a comparative study. Lithos 77, 225–242.

Sobolev, N.V., Logvinova, A.M., Efimova, E.S., 2009. Syngenetic phlogopite inclusions in kimberlite-hosted diamonds: implications for role of volatiles in diamond formation. Russian Geology and Geophysics 50, 1234–1248.

Solov'eva, L.V., Egorov, K.N., Markova, M.E., Kharkiv, A.D., Popolitov, K.E., Barankevich, V.G., 1997. Mantle metasomatism and melting in deep-seated xenoliths from the Udachnaya pipe, their possible relationship with diamond and kimberlite formation. Russian Geology and Geophysics 38 (1), 172–193.

Solov'eva, L.V., Yasnygina, T.A., Egorov, K.N., 2012. Metasomatic parageneses in deep-seated xenoliths from pipes Udachnaya and Komsomol'skaya-Magnitnaya as indicators of fluid transfer through the mantle lithosphere of the Siberian craton. Russian Geology and Geophysics 53, 1304–1323.

Spetsius, Z.V., 2007. In: Vladykin Irkutsk, N.V. (Ed.), The Nature of Indicator Minerals in Kimberlites: A Case from the Mantle Xenoliths Studying. Plumes and Their Sources. Institute of Geography, pp. 90–108.

Spetsius, Z.V., Koptil, V.I., 2008. Associations with the diamond from the kimberlite pipe Sytykanskaya, Yakutia. Geologiya I Razvedka 23–28.

Spetsius, Z.V., Serenko, V.P., 1990. Composition of the Continental Mantle and Low Crustbeneath the Siberian Platform. Nauka, Moscow, p. 271 (in Russian).

Stagno, V., Frost, D.J., 2010. Carbon speciation in the asthenosphere: experimental measurements of the redox conditions at which carbonate - bearing melts coexist with graphite or diamond in peridotite assemblages. Earth and Planetary Science Letters 300, 72–84.

Please cite this article in press as: Ashchepkov, I.V., et al., The Sytykanskaya kimberlite pipe: Evidence from deep-seated xenoliths and xenocrysts for the evolution of the mantle beneath Alakit, Yakutia, Russia, Geoscience Frontiers (2014), http://dx.doi.org/10.1016/j.gsf.2014.08.005

Stagno, V., Ojwang, D.O., McCammon, C.A., Frost, D.J., 2013. The oxidation state of the mantle and the extraction of carbon from Earth's interior. Nature 493, 84–88.

Sweeney, R.J., Thompson, A.B., Ulmer, P., 1993. Phase relations of a natural MARID composition and implications for MARID genesis, lithospheric melting and mantle metasomatism. Contributions to Mineralogy and Petrology 115, 225–241.

Tappe, S., Foley, S.F., Jenner, G.A., Heaman, L.M., Kjarsgaard, B.A., Romer, R.L., Stracke, A., Joyce, N., Hoefs, J., 2006. Genesis of ultramafic lamprophyres and carbonatites at Aillik Bay, Labrador: a consequence of incipient lithospheric thinning beneath the North Atlantic craton. Journal of Petrology 47, 1261–1315.

Taylor, L.A., Anand, M., 2004. Diamonds: time capsules from the Siberian Mantle. Chemie der Erde 64, 1–74.

Taylor, W.R., Kammerman, M., Hamilton, R., 1998. New thermometer and oxygen fugasity sensor calibrations for ilmenite and chromian spinel-bearing peridotitic assemblages. In: 7th International Kimberlite Conference. Extended Abstracts. Cape Town, pp. 891–901.

Travin, A.V., Aschepkov, I.V., Udin, D., Prostyakov, K., 2002. Laser and stepwise-heating $^{40}Ar/^{39}Ar$ dating of kimberlite-like rocks from Sayan Foothills and peripheral part of the Siberian platform. Geochimica et Cosmochimica Acta. Special Supplement 6 (15A), A783.

Travin, A.V., Yudin, D.S., Vladimirov, A.G., Khromykh, S.V., Volkova, N.I., Mekhonoshin, A.S., Kolotilina, T.B., 2009. Thermochronology of the Chernorud granulite zone, Ol'khon Region, Western Baikal area. Geochemistry International 47 (11), 1107–1124.

Zack, T., Brumm, R., 1998. Ilmenite/liquid partition coefficients of 26 trace elements determined through ilmenite/clinopyroxene partitioning in garnet pyroxenite. In: Gurney, J.J., Gurney, J.L., Pascoe, M.D., Richardson, S.H. (Eds.), 7th International Kimberlite Conference. Red Roof Design, Capetown, pp. 986–988.

Ziberna, L., Nimis, P., Zanetti, A., Marzoli, A., Sobolev, N.V., 2013. Metasomatic processes in the Central Siberian Cratonic Mantle: evidence from garnet xenocrysts from the Zagadochnaya Kimberlite. Journal of Petrology 54, 2379–2409.

Please cite this article in press as: Ashchepkov, I.V., et al., The Sytykanskaya kimberlite pipe: Evidence from deep-seated xenoliths and xenocrysts for the evolution of the mantle beneath Alakit, Yakutia, Russia, Geoscience Frontiers (2014), http://dx.doi.org/10.1016/j.gsf.2014.08.005